ACADEMIC PRESS

Available online at www.sciencedirect.com

SCIENCE DIRECT®

Journal of Magnetic Resonance 158 (2002) 99–125

JMR Journal of Magnetic Resonance

www.academicpress.com

Anisotropic relaxation and motion of half-integer quadrupole nuclei studied by central transition nuclear magnetic resonance spectroscopy

Jørgen Holm Kristensen and Ian Farnan*

Department of Earth Sciences, University of Cambridge, Downing Street, Cambridge CB2 3EQ, UK

Received 3 April 2002; revised 11 July 2002

Abstract

An efficient theoretical formalism and advanced experimental methods are presented for studying the effects of anisotropic molecular motion and relaxation on solid-state central transition NMR spectra of half-integer quadrupole nuclei. The theoretical formalism is based on density operator algebra and involves the stochastic Liouville–von Neumann equation. In this approach the nuclear spin interactions are represented by the Hamiltonian while the motion is described by a discrete stochastic operator. The nuclear spin interactions fluctuate randomly in the presence of molecular motion. These fluctuations may stimulate the relaxation of the system and are represented by a discrete relaxation operator. This is derived from second-order perturbation theory and involves the spectral densities of the system. Although the relaxation operator is valid only for small time intervals it may be used recursively to obtain the density operator at any time. The spectral densities are allowed to be explicitly time dependent making the approach valid for all motional regimes. The formalism has been applied to simulate partially relaxed central transition ^{17}O NMR spectra of representative model systems. The results have revealed that partially relaxed central transition lineshapes are defined not only by the nuclear spin interactions but also by anisotropic motion and relaxation. This has formed the basis for the development of central transition spin-echo and inversion-recovery NMR experiments for investigating molecular motion in solids. As an example we have acquired central transition spin-echo and inversion-recovery ^{17}O NMR spectra of polycrystalline cristobalite (SiO_2) at temperatures both below and above the α–β phase transition. It is found that the oxygen atoms exhibit slow motion in α-cristobalite. This motion has no significant effects on the fully relaxed lineshapes but may be monitored by studying the partially relaxed spectra. The α–β phase transition is characterized by structural and motional changes involving a slight increase in the Si–O–Si bond angle and a substantial increase in the mobility of the oxygen atoms. The increase in the Si–O–Si angle is supported by the results of ^{17}O and ^{29}Si NMR spectroscopy. The oxygen motion is shown to be orders of magnitude faster in β-cristobalite resulting in much faster relaxation and characteristic lineshapes. The measured oscillation frequencies are consistent with the rigid unit mode model. This shows that solid-state NMR and lattice dynamics simulations agree and may be used in combination to provide more detailed models of solid materials.

Keywords: Half-integer quadrupole nuclei; Anisotropic relaxation and motion; Density operator algebra; Central transition inversion-recovery spectroscopy; Oxygen disorder in α- and β-cristobalite

1. Introduction

The importance of measuring and characterizing anisotropic motion in condensed matter is becoming increasingly evident as more detailed models of solid materials are being developed. The effects of molecular motion have been observed in many technologically important materials including organic and inorganic polymers [1,2], crystalline and amorphous silicates and aluminosilicates [3], inorganic glasses and melts [4,5], modified silica surfaces [6,7], liquid crystals [8,9], and inclusion compounds [10–12]. An important objective of modern materials science research is to determine the fundamental relations between molecular structure and motion and the observable properties of solids including

* Corresponding author.
E-mail address: ifarnan@esc.cam.ac.uk (I. Farnan).

1090-7807/02/$ - see front matter © 2002 Elsevier Science (USA). All rights reserved.
PII: S1090-7807(02)00065-4

their mechanical and thermodynamic properties, electric and magnetic characteristics, optical properties, catalytic activities, and radiation sensitivity. This may eventually form the basis for the development of new improved materials of interest to science and industry and make it easier to understand and predict different natural phenomena such as magma flow and plate tectonics as well as other geophysical processes that are known to depend on molecular structure and mobility.

There are a variety of experimental and theoretical methods available for investigating the structure of solids among which diffraction techniques represent the most widely used approach for studying crystalline materials [13,14]. However, it is known that diffraction methods and most other techniques are either insensitive to molecular motion or provide only limited information about the details of the system. In order to investigate anisotropic motion it is useful to implement the technique of solid-state nuclear magnetic resonance (NMR) spectroscopy [15,16]. The primary advantage of this method is that it can be applied to structurally and motionally disordered systems such as amorphous polymers and glasses that cannot easily be investigated by diffraction techniques. The method is highly sensitive to the local molecular structure around the nuclei and to structural distributions whereas diffraction techniques depend on the existence of long-range order. This allows a much more detailed investigation of many systems for which there is no long-range order but where structural or motional disorder is important for determining the physical properties.

The most important feature of solid-state NMR is that the spectra are defined by several different nuclear spin interactions including the dipole, quadrupole, and shielding interactions [15,16]. These depend on the molecular structure and chemical bonding making the technique useful for structural investigations. Moreover, the spectra are sensitive to time-dependent phenomena such as molecular motion and relaxation and may provide information about dynamic disorder in condensed matter. The structural and motional NMR parameters may be extracted by simulating the spectra using a physical model of the nuclear spin interactions and the motion. The structural NMR parameters may often be correlated with coordination numbers, bond angles, and bond lengths. Similarly, the motional NMR parameters may be related to different intra- and intermolecular interactions. The usefulness of the method has increased following recent advances in electron structure simulations which have made it possible to predict the structural NMR parameters for different solid materials [17–19]. Similarly, the results of molecular dynamics calculations and Monte Carlo simulations may be used in conjunction with solid-state NMR to probe the dynamic nature of condensed matter [20]. This combination of theoretical and experimental techniques is a promising research area that may provide more detailed models of solid materials.

There is an extensive literature on the simulation of solid-state NMR spectra for almost any nuclear spin system and the determination of structural NMR parameters from experimental spectra has become an important and widely used method for investigating condensed matter [15,16]. However, for motionally disordered systems the progress has been slower and previous investigations have almost exclusively focused on using relatively simple nuclei such as deuterons as probes of molecular motion. The most successful methods for investigating anisotropic motion in solids involve simulating the lineshapes of fully or partially relaxed spectra. In the case of fully relaxed spectra the lineshapes are defined by the anisotropic nuclear spin interactions and the motion [21]. The most important difficulty in simulating molecular motion is that it is often possible to define several different motional models that produce similar fully relaxed lineshapes making it difficult or impossible to interpret the spectra. In the case of partially relaxed systems the spectra are determined not only by the anisotropic nuclear spin interactions and the motion but also by the relaxation anisotropy [22–25]. These effects combine to produce characteristic lineshapes of partially relaxed spectra. The additional information found in the relaxation anisotropy may help in differentiating between models that produce similar fully relaxed spectra. However, it is important to understand that the technique has some limitations and that there may often be several different models for which the partially relaxed lineshapes are indistinguishable. The most obvious advantage of studying partially relaxed spectra is that the number of possible models is reduced significantly. By evaluating the models against other constraints such as molecular geometry and symmetry it is usually possible to distinguish between different mechanisms and accurately characterize the motion.

An additional advantage of studying partially relaxed spectra is that the range over which the motional NMR parameters may be obtained is extended significantly. The wide range of rate constants over which lineshape effects occur in solids is the result of the magnitude and anisotropy of the nuclear spin interactions. However, most investigations are limited by the requirement that the rate constants are comparable to the width of the spectra. If the rate constants are either much smaller or larger than the width of the spectra the lineshapes are either unaffected by the motion or defined by a motionally averaged nuclear spin interaction. In these cases it is impossible to determine the rate constants from the fully relaxed spectra. However, the nuclear spin interactions fluctuate randomly as a result of molecular motion and may stimulate the relaxation of the system [22–25]. Because nuclear spin transitions occur at radio

frequencies molecular motions in this frequency range are most efficient in relaxing the system. However, there is usually sufficient spectral density at both higher and lower frequencies to stimulate significant relaxation. This makes measurements of anisotropic relaxation sensitive to both slow and fast molecular motions that may have no easily discernible effects on the fully relaxed spectra. Moreover, requiring the effects of the relaxation anisotropy to be reproduced places additional constraints on the rate constants. These observations show that studies of partially relaxed lineshapes are essential for any accurate investigation of molecular motion.

There are several experimental techniques that have proven useful for measuring anisotropic relaxation in solids [9]. The inversion-recovery experiment is among the most versatile methods since it may be applied to any nuclear spin system. The fundamental principle in this technique is to create a nonequilibrium state by inverting the nuclear spin transitions. The state of the nonequilibrium system following a variable relaxation period is monitored by a pulse sequence designed to create and detect observable magnetization. The most elaborate investigations have involved quadrupole nuclei with small quadrupole interactions among which deuterons are particularly attractive. In this case the inversion results in a state ρ_z of rank-one dipole alignment. The evolution of this state is defined by the relaxation time T_z which involves two spectral densities $J_1^{(2)}(\omega_0)$ and $J_2^{(2)}(2\omega_0)$. The spectral densities are sensitive to the details of molecular motion. In order to obtain these it is useful to monitor the relaxation of a state ρ_{z^2} of rank-two quadrupole alignment. The corresponding relaxation time T_{z^2} involves only one spectral density $J_2^{(2)}(2\omega_0)$. This demonstrates that the simultaneous measurement of the relaxation of the rank-one dipole and rank-two quadrupole alignments makes it possible to extract the individual spectral densities.

In the case of half-integer quadrupole nuclei ($I = \frac{3}{2}, \frac{5}{2}, \frac{7}{2}, \frac{9}{2}$) it is possible to implement similar techniques for studying anisotropic relaxation and motion [26]. However, there are several difficulties involved in the description and interpretation of relaxation and motion of half-integer quadrupole nuclei that have not previously been fully recognized. As discussed in this paper the selective excitation of any half-integer quadrupole nucleus creates not only rank-one dipole alignment but also higher rank multipole alignments [27–30]. The amounts of these alignments depend on the equilibrium state of the system and the excitation sequence. For half-integer quadrupole nuclei any selective excitation pulse will transfer all odd-rank multipole alignments $\rho_z, \rho_{z^3}, \ldots, \rho_{z^{2I}}$ including the rank-one dipole alignment into odd-rank multipole alignments and all even-rank multipole alignments ρ_{z^2}, $\rho_{z^4}, \ldots, \rho_{z^{2I-1}}$ including the rank-two quadrupole alignment into even-rank multipole alignments. The relaxation of the odd-rank multipole alignments is defined by $I + \frac{1}{2}$ simultaneous equations while the relaxation of the even-rank multipole alignments is specified by a system of $I - \frac{1}{2}$ equations. This makes it impossible to describe the relaxation in terms of simple exponentials and relaxation times. However, it is important to understand that the amounts of higher rank multipole alignments are vanishing in nonselective experiments on nuclei with small quadrupole interactions in which case the relaxation may be exponential. The creation of higher rank multipole alignments makes exponential relaxation impossible and supports the multiexponential model of relaxation. In this paper the effects of higher rank multipole alignments are included in the description. An advanced formalism based on density operator algebra is developed to calculate the combined effects of anisotropic motion and relaxation. This formalism involves arbitrary molecular motion and may be applied to any nuclear spin system. The theoretical results have formed the basis for the development of experimental techniques to measure anisotropic relaxation and motion of half-integer quadrupole nuclei. These methods are based on selective inversion and subsequent observation of central transition spectra.

In order to demonstrate the usefulness of the theoretical and experimental methods introduced in this paper we have applied central transition spin-echo and inversion-recovery ^{17}O NMR spectroscopy to study the oxygen disorder in the silica (SiO_2) polymorph cristobalite. This system is interesting in the context of anisotropic relaxation because it is difficult to obtain a consistent description of the oxygen motion from the fully relaxed lineshapes. The most important difficulty is that the oxygen motion is either slow or fast depending on the temperature. It is shown that although the motion has no substantial effects on the fully relaxed lineshapes it produces a characteristic relaxation anisotropy that makes it possible to determine the structural and motional NMR parameters. For completeness we have obtained central transition spin-echo and inversion-recovery ^{17}O NMR spectra of cristobalite at temperatures both below and above the α–β phase transition. It is found that the oxygen motion is slow in α-cristobalite and depends only weakly on the temperature. The results represent the first direct experimental evidence of dynamic disorder in α-cristobalite. The oxygen motion becomes faster by orders of magnitude at the α–β phase transition and results in significant averaging of the spectra and substantial changes in the relaxation characteristics. The observations are consistent with previous results and provide compelling evidence that β-cristobalite is dynamically disordered. The structure of α-cristobalite is probed by ^{17}O and ^{29}Si NMR spectroscopy and shown to be almost invariant as a function of temperature. However, at the α–β phase transition the system is found to be subject to

small structural modifications involving an increase in the Si–O–Si angle.

2. Theory

2.1. Density operator description of molecular motion and nuclear spin relaxation

2.1.1. Time evolution of nonequilibrium systems

The most fundamental description of the state of an ensemble of nuclear spin systems is obtained by introducing the density operator $\sigma(t)$ that includes all possible coherences and alignments [31]. In the case of nonequilibrium systems the deviation from thermal equilibrium is defined by the deviation density operator $\rho(t) = \sigma(t) - \sigma_0$ where σ_0 is the equilibrium density operator. In the corresponding Zeeman interaction representation [15] the deviation density operator becomes

$$\tilde{\rho}(t) = F(t_0,t)^{\dagger}\rho(t)F(t_0,t), \tag{1}$$

with the propagator

$$F(t_0,t) = \exp(-\mathrm{i}H_0[t-t_0]) \tag{2}$$

defined by the Zeeman Hamiltonian $H_0 = -\omega_0 I_z$ where $\omega_0 = \gamma B_0$ is the Larmor frequency for a nucleus with gyromagnetic ratio γ subject to a magnetic flux density B_0. The time evolution of the deviation density operator is described by the stochastic Liouville–von Neumann equation [32,33]

$$\frac{\partial}{\partial t}|\tilde{\rho}(t)\rangle = \tilde{A}(t)|\tilde{\rho}(t)\rangle, \tag{3}$$

which includes the coefficient operator

$$\tilde{A}(t) = -\mathrm{i}Ad(\tilde{H}(t)) + \Lambda(t) + \Xi, \tag{4}$$

where

$$\tilde{H}(t) = F(t_0,t)^{\dagger}H(t)F(t_0,t) - \mathrm{i}F(t_0,t)^{\dagger}\frac{\partial}{\partial t}F(t_0,t) \tag{5}$$

represents the Zeeman interaction Hamiltonian, $\Lambda(t)$ the relaxation operator, and Ξ the stochastic operator. The Hamiltonian defines the anisotropic nuclear spin interactions while the stochastic operator specifies the motion of the system. The motion induces random fluctuations in the anisotropic nuclear spin interactions. These fluctuations stimulate the relaxation of the system [22–25] and are represented by the relaxation operator.

The motion is assumed to be described by a stochastic process $\{\xi(t)\,|\,t \geqslant t_0\}$ where the stochastic variable $\xi(t)$ defines the motional state of the ensemble. In the case of a discrete stochastic process the values of $\xi(t)$ are given by $\{\xi_n\,|\,n = 1,\ldots,N\}$ where N is the number of states. It is useful to describe the properties of any nuclear spin ensemble by introducing the Lie group $SU(2I+1)$ and its direct products [34]. For an ensemble subject to a discrete stochastic process the corresponding group generators are represented by $\{I_m(\xi_n)\,|\,m = 1,\ldots,M,\ \ n = 1,\ldots,N\}$ where M is the number of coherences and alignments [33]. The group generators transform according to the adjoint representation

$$\begin{aligned} Ad(I_k(\xi_r))|I_l(\xi_s)\rangle &= |[I_k(\xi_r), I_l(\xi_s)]\rangle \\ &= \delta_{rs}\sum_{m=1}^{M} c_{kl}^{m}|I_m(\xi_r)\rangle, \end{aligned} \tag{6}$$

where c_{kl}^{m} are the structure constants. The orthogonality and completeness of the group generators imply that the Hamiltonian and the deviation density operator may be expanded as

$$\tilde{H}(t) = \sum_{m=1}^{M}\tilde{H}_m(t)I_m = \sum_{m=1}^{M}\sum_{n=1}^{N}\tilde{H}_m(\xi_n,t)I_m(\xi_n), \tag{7}$$

$$\tilde{\rho}(t) = \sum_{m=1}^{M}\tilde{\rho}_m(t)I_m = \sum_{m=1}^{M}\sum_{n=1}^{N}\tilde{\rho}_m(\xi_n,t)I_m(\xi_n), \tag{8}$$

where $I_m = \sum_{n=1}^{N} I_m(\xi_n)$ and the expansion coefficients

$$\tilde{H}_m(t) = \frac{\langle I_m|\tilde{H}(t)\rangle}{\langle I_m|I_m\rangle}, \quad \tilde{H}_m(\xi_n,t) = \frac{\langle I_m(\xi_n)|\tilde{H}(t)\rangle}{\langle I_m(\xi_n)|I_m(\xi_n)\rangle}, \tag{9}$$

$$\tilde{\rho}_m(t) = \frac{\langle I_m|\tilde{\rho}(t)\rangle}{\langle I_m|I_m\rangle}, \quad \tilde{\rho}_m(\xi_n,t) = \frac{\langle I_m(\xi_n)|\tilde{\rho}(t)\rangle}{\langle I_m(\xi_n)|I_m(\xi_n)\rangle}, \tag{10}$$

define the components of the Hamiltonian and the deviation density operator. This representation is useful because the components of the deviation density operator define all possible deviation coherences and alignments.

Following the above results the stochastic Liouville–von Neumann equation (Eq. (3)) is developed by inserting the expansions of the Hamiltonian (Eq. (7)) and the deviation density operator (Eq. (8)) to obtain the linear homogeneous system of coupled first-order differential equations

$$\frac{\partial}{\partial t}\tilde{\rho}_k(\xi_r,t) = \sum_{l=1}^{M}\sum_{s=1}^{N}\tilde{a}_{kl}(\xi_r,\xi_s,t)\tilde{\rho}_l(\xi_s,t), \tag{11}$$

where

$$\tilde{a}_{kl}(\xi_r,\xi_s,t) = \frac{\langle I_k(\xi_r)|\tilde{A}(t)|I_l(\xi_s)\rangle}{\langle I_k(\xi_r)|I_k(\xi_r)\rangle} \tag{12}$$

are the elements of the coefficient matrix. This system is usually solved using a numerical integration method [35]. The most important complication is that the equations may be highly stiff making the numerical solution difficult. The stiffness implies that the integration method must have stiff stability and accuracy characteristics [36]. The elements of the coefficient matrix are developed by inserting the expression of the coefficient operator (Eq. (4)) to obtain

$$\tilde{a}_{kl}(\xi_r,\xi_s,t) = -\mathrm{i}\frac{\langle I_k(\xi_r)|Ad(\tilde{H}(t))|I_l(\xi_s)\rangle}{\langle I_k(\xi_r)|I_k(\xi_r)\rangle} + \frac{\langle I_k(\xi_r)|\Delta(t)|I_l(\xi_s)\rangle}{\langle I_k(\xi_r)|I_k(\xi_r)\rangle} + \frac{\langle I_k(\xi_r)|\Xi|I_l(\xi_s)\rangle}{\langle I_k(\xi_r)|I_k(\xi_r)\rangle}, \tag{13}$$

which when combined with

$$\frac{\langle I_k(\xi_r)|Ad(\tilde{H}(t))|I_l(\xi_s)\rangle}{\langle I_k(\xi_r)|I_k(\xi_r)\rangle} = \delta_{rs}\sum_{m=1}^{M}\tilde{H}_m(\xi_r,t)c_{ml}^k, \tag{14}$$

$$\frac{\langle I_k(\xi_r)|\Delta(t)|I_l(\xi_s)\rangle}{\langle I_k(\xi_r)|I_k(\xi_r)\rangle} = \delta_{rs}\Delta_{kl}(\xi_r,t), \tag{15}$$

$$\frac{\langle I_k(\xi_r)|\Xi|I_l(\xi_s)\rangle}{\langle I_k(\xi_r)|I_k(\xi_r)\rangle} = \delta_{kl}\Xi(\xi_r,\xi_s), \tag{16}$$

leads to the result

$$\tilde{a}_{kl}(\xi_r,\xi_s,t) = -\mathrm{i}\delta_{rs}\sum_{m=1}^{M}\tilde{H}_m(\xi_r,t)c_{ml}^k + \delta_{rs}\Delta_{kl}(\xi_r,t) + \delta_{kl}\Xi(\xi_r,\xi_s), \tag{17}$$

which specify the coefficient matrix in terms of the elements $\tilde{H}_m(\xi_r,t)$ of the interaction Hamiltonian, the elements $\Delta_{kl}(\xi_r,t)$ of the relaxation operator, and the elements $\Xi(\xi_r,\xi_s)$ of the stochastic operator. The form of the stochastic operator depends on the details of the motion. In those cases where the motion may be described by a discrete Markov process [24,33] the matrix elements are

$$\Xi(\xi_m,\xi_n) = k_{nm}, \tag{18}$$

$$\Xi(\xi_m,\xi_m) = -\sum_{n=1}^{N}[1-\delta_{mn}]k_{mn}, \tag{19}$$

where k_{mn} are the rate constants. These elements are related by microscopic reversibility

$$\Xi(\xi_m,\xi_n)P(\xi_n) = \Xi(\xi_n,\xi_m)P(\xi_m), \tag{20}$$

where $P(\xi_m)$ are the equilibrium probabilities of the motional states. This demonstrates that given the equilibrium probabilities it is sufficient to define only one triangular part of the stochastic matrix.

2.1.2. Matrix representation of the relaxation operator

In the presence of molecular motion the interaction Hamiltonian becomes a random operator that may stimulate the relaxation of the nuclear spin ensemble. In the following the description of the relaxation is based on second-order perturbation theory [24,25] with the relaxation operator

$$\Delta(t) = -\int_0^{t-t_0}\langle Ad(\tilde{H}(t))Ad(\tilde{H}(t-\tau))\rangle\,\mathrm{d}\tau, \tag{21}$$

where $\langle Ad(\tilde{H}(t))Ad(\tilde{H}(t-\tau))\rangle$ is the correlation function of the adjoint Hamiltonian. This equation may be transcribed by inserting the expansion of the Hamiltonian (Eq. (7)) to obtain

$$\Delta(t) = \sum_{r=1}^{N}\Delta(\xi_r,t), \tag{22}$$

where

$$\Delta(\xi_r,t) = -\sum_{q_1,q_2=1}^{M}Ad(I_{q_1}(\xi_r))Ad(I_{q_2}(\xi_r)) \times\int_0^{t-t_0}\langle\tilde{H}_{q_1}(t)\tilde{H}_{q_2}(t-\tau)\rangle\,\mathrm{d}\tau \tag{23}$$

are the relaxation operators for the different motional states. The corresponding Hamiltonians are

$$H(\xi_r,t) = H_0(\xi_r) + H_1(\xi_r,t) = H_0(\xi_r) + \sum_{p=1}^{M}H_{1p}(\xi_r,t)I_p(\xi_r), \tag{24}$$

which in the interaction representation (Eq. (5)) become

$$\tilde{H}(\xi_r,t) = \tilde{H}_1(\xi_r,t) = \sum_{p=1}^{M}H_{1p}(\xi_r,t)F(t_0,t)^{\dagger}I_p(\xi_r)F(t_0,t), \tag{25}$$

where

$$F(t_0,t)^{\dagger}I_p(\xi_r)F(t_0,t) = \sum_{q=1}^{M}f_{pq}(t_0,t)I_q(\xi_r) = \sum_{q=1}^{M}\sum_{m=-\infty}^{\infty}f_{pq}^{(m)} \times\exp(\mathrm{i}m\omega_0[t-t_0])I_q(\xi_r) \tag{26}$$

define the transformation of the individual group generators. In this equation the transfer functions have been expanded in the Fourier series

$$f_{pq}(t_0,t) = \sum_{m=-\infty}^{\infty}f_{pq}^{(m)}\exp(\mathrm{i}m\omega_0[t-t_0]), \tag{27}$$

where $f_{pq}^{(m)}$ are time independent expansion coefficients. From these results it becomes evident that

$$\tilde{H}(\xi_r,t) = \sum_{p=1}^{M}\sum_{q=1}^{M}\sum_{m=-\infty}^{\infty}H_{1p}(\xi_r,t)f_{pq}^{(m)} \exp(\mathrm{i}m\omega_0[t-t_0])I_q(\xi_r) = \sum_{q=1}^{M}\tilde{H}_q(\xi_r,t)I_q(\xi_r), \tag{28}$$

where

$$\tilde{H}_q(\xi_r,t) = \sum_{p=1}^{M}\sum_{m=-\infty}^{\infty}H_{1p}(\xi_r,t)f_{pq}^{(m)}\exp(\mathrm{i}m\omega_0[t-t_0]) \tag{29}$$

are the individual components. The above equations may be combined to obtain

$$\Delta(\xi_r,t) = -\sum_{p_1,p_2=1}^{M}\sum_{q_1,q_2=1}^{M}\sum_{m_1,m_2=-\infty}^{\infty} Ad(I_{q_1}(\xi_r)) \times Ad(I_{q_2}(\xi_r))f^{(m_1)}_{p_1q_1}f^{(m_2)}_{p_2q_2} \times \exp(\mathrm{i}[m_1+m_2]\omega_0[t-t_0])j_{p_1p_2}(-m_2\omega_0,t), \tag{30}$$

where the spectral densities

$$j_{p_1p_2}(\omega,t) = \int_0^{t-t_0} g_{p_1p_2}(\tau)\exp(\mathrm{i}\omega\tau)\,\mathrm{d}\tau \tag{31}$$

are defined by the correlation functions $g_{p_1p_2}(\tau) = \langle H_{1p_1}(t)H_{1p_2}(t-\tau)\rangle$. The results may be simplified by restricting to secular terms in which case

$$\Delta(\xi_r,t) = -\sum_{p_1,p_2=1}^{M}\sum_{q_1,q_2=1}^{M}\sum_{m=-\infty}^{\infty} Ad(I_{q_1}(\xi_r)) \times Ad(I_{q_2}(\xi_r))f^{(m)}_{p_1q_1}f^{(-m)}_{p_2q_2}j_{p_1p_2}(m\omega_0,t) \tag{32}$$

and by ignoring small frequency shifts one finds that

$$\Delta(\xi_r,t) = -\frac{1}{2}\sum_{p_1,p_2=1}^{M}\sum_{q_1,q_2=1}^{M}\sum_{m=-\infty}^{\infty} Ad(I_{q_1}(\xi_r)) \times Ad(I_{q_2}(\xi_r))f^{(m)}_{p_1q_1}f^{(-m)}_{p_2q_2}J_{p_1p_2}(m\omega_0,t), \tag{33}$$

where the spectral densities

$$J_{p_1p_2}(\omega,t) = 2\int_0^{t-t_0} g_{p_1p_2}(\tau)\cos(\omega\tau)\,\mathrm{d}\tau \tag{34}$$

are real and even functions. The matrix elements of the relaxation operator (Eq. (15)) are

$$\Delta_{kl}(\xi_r,t) = -\frac{1}{2}\sum_{p_1,p_2=1}^{M}\sum_{q_1,q_2=1}^{M}\sum_{m=-\infty}^{\infty} \times \frac{\langle I_k(\xi_r)|Ad(I_{q_1}(\xi_r))Ad(I_{q_2}(\xi_r))|I_l(\xi_r)\rangle}{\langle I_k(\xi_r)|I_k(\xi_r)\rangle} \times f^{(m)}_{p_1q_1}f^{(-m)}_{p_2q_2}J_{p_1p_2}(m\omega_0,t), \tag{35}$$

which may be rewritten to obtain

$$\Delta_{kl}(\xi_r,t) = -\frac{1}{2}\sum_{p_1,p_2=1}^{M}\sum_{q_1,q_2=1}^{M}\sum_{q_3=1}^{M}\sum_{m=-\infty}^{\infty} \times c^{k}_{q_1q_3}c^{q_3}_{q_2l}f^{(m)}_{p_1q_1}f^{(-m)}_{p_2q_2}J_{p_1p_2}(m\omega_0,t), \tag{36}$$

where we have used the transformation properties (Eq. (6)) of the group generators. Although this formalism is valid only for small time intervals where $\Delta_{kl}(\xi_r,t)[t-t_0] \ll 1$ it may be implemented recursively to obtain the deviation density operator at any time.

2.1.3. Evaluation of correlation functions

The elements of the relaxation operator are specified by the spectral densities of the fluctuating magnetic interactions generated by the motion. In the previous section it was shown that the spectral densities are defined by the corresponding correlation functions. In order to determine the form of these we consider the Hamiltonian elements $H_{1p}(t) = H_{1p}(\xi(t),t)$ where the time dependence has been separated into a contribution from the stochastic process $\{\xi(t)|t \geqslant t_0\}$ and a contribution from any coherent interaction. The correlation functions $g_{p_1p_1}(\tau) = \langle H_{1p_1}(t)H_{1p_2}(t+\tau)\rangle$ are given by [22–25]

$$\langle H_{1p_1}(t)H_{1p_2}(t+\tau)\rangle = \sum_{k=1}^{N}\sum_{l=1}^{N} H_{1p_1}(\xi_l,t)H_{1p_2}(\xi_k,t+\tau)^* \times P(\xi_l)P(\xi_k,t+\tau|\xi_l,t), \tag{37}$$

where $P(\xi_k,t+\tau|\xi_l,t)$ is the conditional probability that the stochastic variable $\xi(t)$ has the value ξ_k at time $t+\tau$ given it had the value ξ_l at time t. It is evident that $g_{p_1p_2}(\tau) = g_{p_1p_2}(-\tau) = g_{p_2p_1}(\tau)^*$ define the fundamental symmetry of the correlation functions. In the case of a discrete Markov process the conditional probabilities obey the equation

$$\frac{\partial}{\partial\tau}\mathbf{P}(\tau) = \mathbf{\Xi}\mathbf{P}(\tau), \tag{38}$$

where the matrices $\mathbf{P}(\tau) = \{P(\xi_k,t+\tau|\xi_l,t\}$ and $\mathbf{\Xi} = \{\Xi(\xi_k,\xi_l)\}$. The solution is expressed by

$$\mathbf{P}(\tau) = \exp(\mathbf{\Xi}\tau), \tag{39}$$

which involves an explicit matrix exponential. The stochastic matrix may be symmetrized by the transformation $\mathbf{S}^{-1}\mathbf{\Xi}\mathbf{S}$ where the diagonal matrix $\mathbf{S} = \{S_{kl}\} = \{P(\xi_k)^{1/2}\delta_{kl}\}$ is defined by the equilibrium probabilities [21]. The symmetrized system satisfies the equation $\mathbf{T}^{-1}\mathbf{S}^{-1}\mathbf{\Xi}\mathbf{S}\mathbf{T} = \mathbf{\Lambda}$ where $\mathbf{T} = \{T_{kl}\}$ is the eigenvector matrix and $\mathbf{\Lambda} = \{\lambda_k\delta_{kl}\}$ the eigenvalue matrix. These results lead to

$$P(\xi_k,t+\tau|\xi_l,t) = \sum_{m=1}^{N} S_{kk}S^{-1}_{ll}T_{km}T_{lm}\exp(\lambda_m\tau), \tag{40}$$

which allows the correlation functions to be rewritten in the form

$$\langle H_{1p_1}(t)H_{1p_2}(t+\tau)\rangle = \sum_{k=1}^{N}\sum_{l=1}^{N}\sum_{m=1}^{N} H_{1p_1}(\xi_l,t) \times H_{1p_2}(\xi_k,t+\tau)^* b^{(m)}_{kl}\exp(\lambda_m\tau), \tag{41}$$

where $b^{(m)}_{kl} = S_{kk}S_{ll}T_{km}T_{lm}$ are time independent coefficients. It is straightforward to show that the eigenvalues are real and negative for the stochastic matrix. This implies that the correlation functions are a weighed sum of decaying exponentials. The corresponding spectral densities are

$$J_{p_1p_2}(\omega,t) = 2\sum_{k=1}^{N}\sum_{l=1}^{N}\sum_{m=1}^{N}\int_0^{t-t_0} H_{1p_1}(\xi_l,t) \times H_{1p_2}(\xi_k,t+\tau)^* b^{(m)}_{kl}\exp(\lambda_m\tau)\cos(\omega\tau)\,\mathrm{d}\tau, \tag{42}$$

where any time dependence of the elements of the Hamiltonian must be considered explicitly. In the case of fast motion the correlation times become very small allowing the upper limit of the integral to be extended to infinity [24,25]. This makes the spectral densities become time independent and simplifies the description of the relaxation process.

2.1.4. Representation by irreducible tensor operators

The relaxation formalism developed above may be implemented for any set of group generators and any nuclear spin interaction. The group generators are selected primarily on the basis of the symmetry and selectivity of the coherence transfer pathways. For nonselective and nonsymmetric coherence transfer pathways the description is simplified by implementing irreducible $SU(2)$ tensor operators for $SU(2I+1)$ [34]. In this case the interaction Hamiltonians may be expressed in the form

$$H_1(\xi_r,t)=\sum_k\sum_m(-1)^m S(I,k)^2 A^{(k)}_{-m}(\xi_r,t)T^{(k)}_m(\xi_r), \quad (43)$$

where the normalization factors

$$S(I,k)=k!\sqrt{\frac{12[2I+k+1]![2I-1]!}{[2I-k]![2k]![2I+2]![2k+1]2^k}} \quad (44)$$

have been chosen so that the norm is independent of the rank k and identical to

$$\left\langle T^{(k_1)}_{m_1}(\xi_r)|T^{(k_2)}_{m_2}(\xi_r)\right\rangle=\tfrac{1}{3}I[I+1][2I+1]\delta_{k_1k_2}\delta_{m_1m_2}, \quad (45)$$

which only depends on the spin quantum number I. This normalization is particularly attractive because it guarantees that all coherence transfer functions and spectral densities exhibit maximum symmetry while retaining the transformation properties of the tensor operators. The interaction representation is readily obtained by implementing the equation

$$F(t_0,t)^\dagger T^{(k)}_m(\xi_r)F(t_0,t)=\exp(-\mathrm{i}m\omega_0[t-t_0])T^{(k)}_m(\xi_r), \quad (46)$$

which leads to the relaxation operators

$$\Delta(\xi_r,t)=-\frac{1}{2}\sum_k\sum_m S(I,k)^4 \times Ad(T^{(k)}_m(\xi_r))Ad(T^{(k)}_{-m}(\xi_r))J^{(k)}_m(m\omega_0,t), \quad (47)$$

where the spectral densities

$$J^{(k)}_m(\omega,t)=2\int_0^{t-t_0}g^{(k)}_m(\tau)\cos(\omega\tau)\,\mathrm{d}\tau \quad (48)$$

involve the correlation functions $g^{(k)}_m(\tau)=\langle A^{(k)}_{-m}(t)A^{(k)}_m(t-\tau)\rangle$. The matrix elements of the relaxation operator are

$$\Delta^{(k_1k_3)}_{m_1m_3}(\xi_r,t)=-\frac{1}{2}\sum_k\sum_{m_2}S(I,k_2)^4 \times\frac{\langle T^{(k_1)}_{m_1}(\xi_r)|Ad(T^{(k_2)}_{m_2}(\xi_r))Ad(T^{(k_2)}_{-m_2}(\xi_r))|T^{(k_3)}_{m_3}(\xi_r)\rangle}{\langle T^{(k_1)}_{m_1}(\xi_r)|T^{(k_1)}_{m_1}(\xi_r)\rangle} \times J^{(k_2)}_{m_2}(m_2\omega_0,t), \quad (49)$$

which define a system of simultaneous equations among the alignments and coherences. In the case of nonselective and symmetric coherence transfer pathways it is more convenient to use the irreducible cartesian $SU(2)$ tensor operators for $SU(2I+1)$ [34]. These involve symmetric and antisymmetric combinations of irreducible $SU(2)$ tensor operators and are defined by

$$\mathbf{I}^{(k)}(\xi_r)=\left\{\frac{1}{\sqrt{2}}\left[T^{(k)}_{-m}(\xi_r)+(-1)^m T^{(k)}_m(\xi_r)\right], T^{(k)}_0(\xi_r),\frac{\mathrm{i}}{\sqrt{2}}\left[T^{(k)}_m(\xi_r)-(-1)^m T^{(k)}_{-m}(\xi_r)\right]\right\}, \quad (50)$$

where the individual elements are Hermitian. The interaction Hamiltonians may be expressed in terms of irreducible cartesian $SU(2)$ tensor operators by the equation

$$H_1(\xi_r,t)=\sum_k\sum_m S(I,k)^2 A^{(k)}_m(\xi_r,t)I^{(k)}_m(\xi_r), \quad (51)$$

where the individual components are identified by the rank and corresponding cartesian harmonic homogeneous polynomial. An important advantage of these representations is that the form and transformation properties of the Hamiltonians are described more easily. This is useful in NMR spectroscopy where the Hamiltonians are often transformed between different coordinate systems.

2.1.5. The nuclear spin Hamiltonian

The interaction of any single nuclear spin system involves several different contributions and is represented by the Hamiltonian

$$H_1(\xi_r,t)=H_{\mathrm{rf}}(\xi_r,t)+H_{\mathrm{S}}(\xi_r,t)+H_{\mathrm{Q}}(\xi_r,t), \quad (52)$$

where $H_{\mathrm{rf}}(\xi_r,t)$ defines the interaction with external radio frequency (rf) fields, $H_{\mathrm{S}}(\xi_r,t)$ represents the shielding interaction, and $H_{\mathrm{Q}}(\xi_r,t)$ specifies the quadrupole interaction. For most quadrupole nuclei the shielding and quadrupole interactions are substantial and must be considered during periods of rf irradiation. The shielding and quadrupole interactions influence the coherence transfer functions and may produce significant intensity and phase distortions in the calculated lineshapes. These effects are especially pronounced in selective experiments using weak rf irradiation and long rf pulses.

The rf field Hamiltonian describes the coupling between the nuclear dipole moment and any external oscillating magnetic flux density. The interaction is conveniently expressed in terms of irreducible cartesian tensor operators according to [15,34]

$$H_{\mathrm{rf}}(\xi_r,t) = \langle \mathbf{A}_{\mathrm{rf}}^{(1)}(t) \,|\, \mathbf{I}_{\mathrm{rf}}^{(1)}(\xi_r)\rangle, \tag{53}$$

where $\mathbf{A}_{\mathrm{rf}}^{(1)}(t) = -2\gamma\mathbf{B}_{\mathrm{rf}}(t)$ and $\mathbf{I}_{\mathrm{rf}}^{(1)}(\xi_r) = \mathbf{I}^{(1)}(\xi_r)$ are the first-rank irreducible cartesian rf field tensors for a nucleus with gyromagnetic ratio γ. The magnetic rf flux density $\mathbf{B}_{\mathrm{rf}}(t) = -B_{\mathrm{rf}}\cos(\omega t)\mathbf{e}_{\mathrm{rf}}$ is defined by its magnitude B_{rf}, angular frequency ω, and direction $\mathbf{e}_{\mathrm{rf}} = \{\cos(\varphi), \sin(\varphi), 0\}$ where φ specifies the phase of the rf field. In the Zeeman interaction representation the first-order average rf field Hamiltonian is

$$\tilde{H}_{\mathrm{rf}}^{(1)}(\xi_r) = \omega_{\mathrm{rf}}\big[I_x(\xi_r)\cos(\varphi) + I_y(\xi_r)\sin(\varphi)\big], \tag{54}$$

where $\omega_{\mathrm{rf}} = \gamma B_{\mathrm{rf}}$ is the angular rf field strength. Because of its relatively small magnitude the rf field Hamiltonian must usually be combined with the shielding and quadrupole interactions to accurately represent the effects of rf irradiation on both fully and partially relaxed lineshapes.

The shielding Hamiltonian describes the electron modulated interaction between the nuclear dipole moment and the external magnetic flux density. This effect depends on the electronic state and may be used to obtain structural information about the system. The shielding Hamiltonian is given by [15,34]

$$H_{\mathrm{S}}(\xi_r,t) = S(I,1)^2\left\langle \mathbf{A}_{\mathrm{S}}^{(1)}(\xi_r,t)\,\middle|\,\mathbf{I}_{\mathrm{S}}^{(1)}(\xi_r)\right\rangle + S(I,2)^2\left\langle \mathbf{A}_{\mathrm{S}}^{(2)}(\xi_r,t)\,\middle|\,\mathbf{I}_{\mathrm{S}}^{(2)}(\xi_r)\right\rangle, \tag{55}$$

where the first-rank irreducible cartesian shielding tensors

$$\mathbf{A}_{\mathrm{S}}^{(1)}(\xi_r,t) = \left\{A_x^{\mathrm{S}}(\xi_r,t), A_z^{\mathrm{S}}(\xi_r,t), A_y^{\mathrm{S}}(\xi_r,t)\right\}, \tag{56}$$

$$\mathbf{I}_{\mathrm{S}}^{(1)}(\xi_r) = \left\{I_x^{\mathrm{S}}(\xi_r), I_z^{\mathrm{S}}(\xi_r), I_y^{\mathrm{S}}(\xi_r)\right\}, \tag{57}$$

and the second-rank irreducible cartesian shielding tensors

$$\mathbf{A}_{\mathrm{S}}^{(2)}(\xi_r,t) = \left\{A_{x^2-y^2}^{\mathrm{S}}(\xi_r,t), A_{xz}^{\mathrm{S}}(\xi_r,t), A_{z^2}^{\mathrm{S}}(\xi_r,t), A_{yz}^{\mathrm{S}}(\xi_r,t), A_{xy}^{\mathrm{S}}(\xi_r,t)\right\}, \tag{58}$$

$$\mathbf{I}_{\mathrm{S}}^{(2)}(\xi_r) = \left\{I_{x^2-y^2}^{\mathrm{S}}(\xi_r), I_{xz}^{\mathrm{S}}(\xi_r), I_{z^2}^{\mathrm{S}}(\xi_r), I_{yz}^{\mathrm{S}}(\xi_r), I_{xy}^{\mathrm{S}}(\xi_r)\right\}, \tag{59}$$

are defined in Tables 1 and 2 in terms of the cartesian tensor components. For a nonrotating sample the irreducible cartesian shielding tensors may be obtained from

$$\langle \mathbf{A}_{\mathrm{S}}^{(1)}(\xi_r)| = \langle \mathbf{a}_{\mathrm{S}}^{(1)}(\xi_r)|\mathbf{\Gamma}^{(1)}(\mathbf{\Omega}_1(\xi_r))\mathbf{\Gamma}^{(1)}(\mathbf{\Omega}_2(\xi_r))\mathbf{\Gamma}^{(1)}(\mathbf{\Omega}_3), \tag{60}$$

Table 1
Components of the first-rank irreducible cartesian shielding tensor

$$A_x^{\mathrm{S}}(\xi_r,t) = \frac{\mathrm{i}}{\sqrt{2}S(I,1)}[S_{zy}(\xi_r,t) - S_{yz}(\xi_r,t)]$$

$$A_z^{\mathrm{S}}(\xi_r,t) = \frac{\mathrm{i}}{\sqrt{2}S(I,1)}[S_{yx}(\xi_r,t) - S_{xy}(\xi_r,t)]$$

$$A_y^{\mathrm{S}}(\xi_r,t) = \frac{\mathrm{i}}{\sqrt{2}S(I,1)}[S_{xz}(\xi_r,t) - S_{zx}(\xi_r,t)]$$

$$I_x^{\mathrm{S}}(\xi_r) = \frac{\mathrm{i}\gamma}{\sqrt{2}S(I,1)}[I_z(\xi_r)B_{0y} - I_y(\xi_r)B_{0z}]$$

$$I_z^{\mathrm{S}}(\xi_r) = \frac{\mathrm{i}\gamma}{\sqrt{2}S(I,1)}[I_y(\xi_r)B_{0x} - I_x(\xi_r)B_{0y}]$$

$$I_y^{\mathrm{S}}(\xi_r) = \frac{\mathrm{i}\gamma}{\sqrt{2}S(I,1)}[I_x(\xi_r)B_{0z} - I_z(\xi_r)B_{0x}]$$

$$\langle \mathbf{A}_{\mathrm{S}}^{(2)}(\xi_r)| = \langle \mathbf{a}_{\mathrm{S}}^{(2)}(\xi_r)|\mathbf{\Gamma}^{(2)}(\mathbf{\Omega}_1(\xi_r))\mathbf{\Gamma}^{(2)}(\mathbf{\Omega}_2(\xi_r))\mathbf{\Gamma}^{(2)}(\mathbf{\Omega}_3), \tag{61}$$

where $\mathbf{\Gamma}^{(1)}(\mathbf{\Omega})$ and $\mathbf{\Gamma}^{(2)}(\mathbf{\Omega})$ define the first- and second-rank irreducible cartesian representation matrices [34]. The transformation from the principal axis system of the shielding tensor to the principal axis system of the

Table 2
Components of the second-rank irreducible cartesian shielding tensor

$$A_{x^2-y^2}^{\mathrm{S}}(\xi_r,t) = \frac{1}{\sqrt{2}S(I,2)}[S_{xx}(\xi_r,t) - S_{yy}(\xi_r,t)]$$

$$A_{xz}^{\mathrm{S}}(\xi_r,t) = \frac{1}{\sqrt{2}S(I,2)}[S_{xz}(\xi_r,t) + S_{zx}(\xi_r,t)]$$

$$A_{z^2}^{\mathrm{S}}(\xi_r,t) = \frac{1}{\sqrt{6}S(I,2)}[2S_{zz}(\xi_r,t) - S_{xx}(\xi_r,t) - S_{yy}(\xi_r,t)]$$

$$A_{yz}^{\mathrm{S}}(\xi_r,t) = \frac{1}{\sqrt{2}S(I,2)}[S_{yz}(\xi_r,t) + S_{zy}(\xi_r,t)]$$

$$A_{xy}^{\mathrm{S}}(\xi_r,t) = -\frac{1}{\sqrt{2}S(I,2)}[S_{xy}(\xi_r,t) + S_{yx}(\xi_r,t)]$$

$$I_{x^2-y^2}^{\mathrm{S}}(\xi_r) = \frac{\gamma}{\sqrt{2}S(I,2)}[I_x(\xi_r)B_{0x} - I_y(\xi_r)B_{0y}]$$

$$I_{xz}^{\mathrm{S}}(\xi_r) = \frac{\gamma}{\sqrt{2}S(I,2)}[I_x(\xi_r)B_{0z} + I_z(\xi_r)B_{0x}]$$

$$I_{z^2}^{\mathrm{S}}(\xi_r) = \frac{\gamma}{\sqrt{6}S(I,2)}[2I_z(\xi_r)B_{0z} - I_x(\xi_r)B_{0x} - I_y(\xi_r)B_{0y}]$$

$$I_{yz}^{\mathrm{S}}(\xi_r) = \frac{\gamma}{\sqrt{2}S(I,2)}[I_y(\xi_r)B_{0z} + I_z(\xi_r)B_{0y}]$$

$$I_{xy}^{\mathrm{S}}(\xi_r) = -\frac{\gamma}{\sqrt{2}S(I,2)}[I_x(\xi_r)B_{0y} + I_y(\xi_r)B_{0x}]$$

quadrupole tensor is specified by the set of Euler angles $\mathbf{\Omega}_1(\xi_r)$ whereas $\mathbf{\Omega}_2(\xi_r)$ defines the relative orientation of the principal axis system of the quadrupole tensor and the crystallite fixed axis system. The set $\mathbf{\Omega}_3$ specifies the transformation from the crystallite to laboratory fixed axis system. In the principal axis system the irreducible cartesian shielding tensors are [34]

$$\mathbf{a}_{\mathrm{S}}^{(1)}(\xi_r) = \frac{\mathrm{i}\sqrt{2}}{S(I,1)}\Big\{-\Lambda_{yz}^{\mathrm{S}}(\xi_r), -\Lambda_{xy}^{\mathrm{S}}(\xi_r), \Lambda_{xz}^{\mathrm{S}}(\xi_r)\Big\}, \tag{62}$$

$$\mathbf{a}_{\mathrm{S}}^{(2)}(\xi_r) = \frac{C_{\mathrm{S}}(\xi_r)}{\sqrt{2}S(I,2)}\Big\{-\eta_{\mathrm{S}}(\xi_r), 0, \sqrt{3}, 0, 0\Big\}, \tag{63}$$

where the shielding constant $C_{\mathrm{S}}(\xi_r)$ and asymmetry parameter $\eta_{\mathrm{S}}(\xi_r)$ are defined by

$$C_{\mathrm{S}}(\xi_r) = \Lambda_{zz}^{\mathrm{S}}(\xi_r) - S_{\mathrm{iso}}(\xi_r), \tag{64}$$

$$\eta_{\mathrm{S}}(\xi_r) = \frac{\Lambda_{yy}^{\mathrm{S}}(\xi_r) - \Lambda_{xx}^{\mathrm{S}}(\xi_r)}{\Lambda_{zz}^{\mathrm{S}}(\xi_r) - S_{\mathrm{iso}}(\xi_r)}, \tag{65}$$

with the principal components $\Lambda_{zz}^{\mathrm{S}}(\xi_r) > \Lambda_{yy}^{\mathrm{S}}(\xi_r) \geqslant \Lambda_{xx}^{\mathrm{S}}(\xi_r)$ or $\Lambda_{zz}^{\mathrm{S}}(\xi_r) < \Lambda_{yy}^{\mathrm{S}}(\xi_r) \leqslant \Lambda_{xx}^{\mathrm{S}}(\xi_r)$ of the shielding tensor and the isotropic shielding $S_{\mathrm{iso}}(\xi_r) = \frac{1}{3}[\Lambda_{xx}^{\mathrm{S}}(\xi_r) + \Lambda_{yy}^{\mathrm{S}}(\xi_r) + \Lambda_{zz}^{\mathrm{S}}(\xi_r)]$. The first-order average shielding Hamiltonian is defined in the Zeeman interaction representation by [34,37]

$$\tilde{H}_{\mathrm{S}}^{(1)}(\xi_r,t) = \left[S(I,2)\sqrt{\frac{2}{3}}\omega_0 A_{z^2}^{\mathrm{S}}(\xi_r,t) + \omega_{\mathrm{iso}}(\xi_r)\right] I_z(\xi_r), \tag{66}$$

where $\omega_{\mathrm{iso}}(\xi_r) = \omega_0 S_{\mathrm{iso}}(\xi_r)$ is the isotropic shielding frequency. This Hamiltonian is sufficient to represent small or moderate shielding effects on fully relaxed lineshapes.

The quadrupole Hamiltonian specifies the interaction between the electric field gradient and the quadrupole moment of the nuclei. The electric field gradient is sensitive to the electronic state making the quadrupole interaction important for structural investigations. The interaction is described by the quadrupole Hamiltonian [15,34]

$$H_{\mathrm{Q}}(\xi_r,t) = S(I,2)^2 \langle \mathbf{A}_{\mathrm{Q}}^{(2)}(\xi_r,t) \,|\, \mathbf{I}_{\mathrm{Q}}^{(2)}(\xi_r)\rangle, \tag{67}$$

where the components of the second-rank irreducible cartesian quadrupole tensors

$$\mathbf{A}_{\mathrm{Q}}^{(2)}(\xi_r,t) = \Big\{A_{x^2-y^2}^{\mathrm{Q}}(\xi_r,t), A_{xz}^{\mathrm{Q}}(\xi_r,t), A_{z^2}^{\mathrm{Q}}(\xi_r,t), A_{yz}^{\mathrm{Q}}(\xi_r,t), A_{xy}^{\mathrm{Q}}(\xi_r,t)\Big\} \tag{68}$$

and $\mathbf{I}_{\mathrm{Q}}^{(2)}(\xi_r) = \mathbf{I}^{(2)}(\xi_r)$ are given in Table 3 in terms of the corresponding cartesian tensor elements. For a non-rotating sample the second-rank irreducible cartesian quadrupole tensor is obtained from

Table 3
Components of the second-rank irreducible cartesian quadrupole tensor

$$A_{x^2-y^2}^{\mathrm{Q}}(\xi_r,t) = \frac{1}{\sqrt{2}S(I,2)}[Q_{xx}(\xi_r,t) - Q_{yy}(\xi_r,t)]$$

$$A_{xz}^{\mathrm{Q}}(\xi_r,t) = \frac{1}{\sqrt{2}S(I,2)}[Q_{xz}(\xi_r,t) + Q_{zx}(\xi_r,t)]$$

$$A_{z^2}^{\mathrm{Q}}(\xi_r,t) = \frac{\sqrt{3}}{\sqrt{2}S(I,2)}Q_{zz}(\xi_r,t)$$

$$A_{yz}^{\mathrm{Q}}(\xi_r,t) = \frac{1}{\sqrt{2}S(I,2)}[Q_{yz}(\xi_r,t) + Q_{zy}(\xi_r,t)]$$

$$A_{xy}^{\mathrm{Q}}(\xi_r,t) = -\frac{1}{\sqrt{2}S(I,2)}[Q_{xy}(\xi_r,t) + Q_{yx}(\xi_r,t)]$$

$$I_{x^2-y^2}^{\mathrm{Q}}(\xi_r) = \frac{1}{\sqrt{2}S(I,2)}[I_x(\xi_r)I_x(\xi_r) - I_y(\xi_r)I_y(\xi_r)]$$

$$I_{xz}^{\mathrm{Q}}(\xi_r) = \frac{1}{\sqrt{2}S(I,2)}[I_x(\xi_r)I_z(\xi_r) + I_z(\xi_r)I_x(\xi_r)]$$

$$I_{z^2}^{\mathrm{Q}}(\xi_r) = \frac{1}{\sqrt{6}S(I,2)}[2I_z(\xi_r)I_z(\xi_r) - I_x(\xi_r)I_x(xi_r) - I_y(\xi_r)I_y(\xi_r)]$$

$$I_{yz}^{\mathrm{Q}}(\xi_r) = \frac{1}{\sqrt{2}S(I,2)}[I_y(\xi_r)I_z(\xi_r) + I_z(\xi_r)I_y(\xi_r)]$$

$$I_{xy}^{\mathrm{Q}}(\xi_r) = -\frac{1}{\sqrt{2}S(I,2)}[I_x(\xi_r)I_y(\xi_r) + I_y(\xi_r)I_x(\xi_r)]$$

$$\langle \mathbf{A}_{\mathrm{Q}}^{(2)}(\xi_r)| = \langle \mathbf{a}_{\mathrm{Q}}^{(2)}(\xi_r)|\mathbf{\Gamma}^{(2)}(\mathbf{\Omega}_2(\xi_r))\mathbf{\Gamma}^{(2)}(\mathbf{\Omega}_3), \tag{69}$$

where the principal second-rank irreducible cartesian quadrupole tensor [34]

$$\mathbf{a}_{\mathrm{Q}}^{(2)}(\xi_r) = \frac{C_{\mathrm{Q}}(\xi_r)}{2\sqrt{2}I[2I-1]S(I,2)}\{-\eta_{\mathrm{Q}}(\xi_r), 0, \sqrt{3}, 0, 0\} \tag{70}$$

involves the quadrupole coupling constant $C_{\mathrm{Q}}(\xi_r)$ and asymmetry parameter $\eta_{\mathrm{Q}}(\xi_r)$ defined by

$$C_{\mathrm{Q}}(\xi_r) = 2I[2I-1]\Lambda_{zz}^{\mathrm{Q}}(\xi_r), \tag{71}$$

$$\eta_{\mathrm{Q}}(\xi_r) = \frac{\Lambda_{yy}^{\mathrm{Q}}(\xi_r) - \Lambda_{xx}^{\mathrm{Q}}(\xi_r)}{\Lambda_{zz}^{\mathrm{Q}}(\xi_r)}, \tag{72}$$

where $\Lambda_{zz}^{\mathrm{Q}}(\xi_r) > \Lambda_{yy}^{\mathrm{Q}}(\xi_r) \geqslant \Lambda_{xx}^{\mathrm{Q}}(\xi_r)$ or $\Lambda_{zz}^{\mathrm{Q}}(\xi_r) < \Lambda_{yy}^{\mathrm{Q}}(\xi_r) \leqslant \Lambda_{xx}^{\mathrm{Q}}(\xi_r)$ are the principal components of the quadrupole tensor. In the Zeeman interaction representation the first- and second-order average quadrupole Hamiltonians are given by [34,37]

$$\tilde{H}_{\mathrm{Q}}^{(1)}(\xi_r,t) = S(I,2)^2 A_{z^2}^{\mathrm{Q}}(\xi_r,t) I_{z^2}(\xi_r), \tag{73}$$

Table 4
Matrix elements of the spin $I = \frac{3}{2}$ quadrupole relaxation operator

$$\Delta^{Q}_{z,z}(\xi_r,t) = -\tfrac{18}{25}[J^{Q}_{xz,xz}(\omega_0,t) + J^{Q}_{yz,yz}(\omega_0,t) + 4J^{Q}_{x^2-y^2,x^2-y^2}(2\omega_0,t) + 4J^{Q}_{xy,xy}(2\omega_0,t)]$$

$$\Delta^{Q}_{z,z^3}(\xi_r,t) = -\tfrac{36}{25}[J^{Q}_{xz,xz}(\omega_0,t) + J^{Q}_{yz,yz}(\omega_0,t) - J^{Q}_{x^2-y^2,x^2-y^2}(2\omega_0,t) - J^{Q}_{xy,xy}(2\omega_0,t)]$$

$$\Delta^{Q}_{z^3,z}(\xi_r,t) = -\tfrac{36}{25}[J^{Q}_{xz,xz}(\omega_0,t) + J^{Q}_{yz,yz}(\omega_0,t) - J^{Q}_{x^2-y^2,x^2-y^2}(2\omega_0,t) - J^{Q}_{xy,xy}(2\omega_0,t)]$$

$$\Delta^{Q}_{z^3,z^3}(\xi_r,t) = -\tfrac{18}{25}[4J^{Q}_{xz,xz}(\omega_0,t) + 4J^{Q}_{yz,yz}(\omega_0,t) + J^{Q}_{x^2-y^2,x^2-y^2}(2\omega_0,t) + J^{Q}_{xy,xy}(2\omega_0,t)]$$

$$\Delta^{Q}_{z^2,z^2}(\xi_r,t) = -\tfrac{18}{5}[J^{Q}_{xz,xz}(\omega_0,t) + J^{Q}_{yz,yz}(\omega_0,t) + J^{Q}_{x^2-y^2,x^2-y^2}(2\omega_0,t) + J^{Q}_{xy,xy}(2\omega_0,t)]$$

$$\tilde{H}^{(2)}_{Q}(\xi_r,t) = \frac{-iS(I,2)^4}{4\omega_0}\sum_{k=1}^{2I}\Big[\Big[A^{Q}_{x^2-y^2}(\xi_r,t)^2 + A^{Q}_{xy}(\xi_r,t)^2\Big]c^{z^k}_{x^2-y^2,xy} + 2\Big[A^{Q}_{xz}(\xi_r,t)^2 + A^{Q}_{yz}(\xi_r,t)^2\Big]c^{z^k}_{yz,xz}\Big]I_{z^k}(\xi_r), \tag{74}$$

where the nondiagonal elements of the second-order average quadrupole interaction have been ignored for simplicity. These Hamiltonians account for most quadrupole effects on fully relaxed spectra.

2.2. Simulation of central transition inversion-recovery spectra

2.2.1. Relaxation of spin $I = \frac{3}{2}$ multipole alignments

In order to obtain complementary information about molecular motion in solids it is useful to study the relaxation of the nuclear spin multipole alignments. For any nuclear spin there are $2I$ multipole alignments defining the polarization of the system. In the case of half-integer quadrupole nuclei these may be classified into $I+\frac{1}{2}$ odd-rank multipole alignments $\rho_z, \rho_{z^3}, \ldots, \rho_{z^{2I}}$ including the rank-one dipole alignment and $I-\frac{1}{2}$ even-rank multipole alignments $\rho_{z^2}, \rho_{z^4}, \ldots, \rho_{z^{2I-1}}$ including the rank-two quadrupole alignment. The most important interactions for half-integer quadrupole nuclei are usually the quadrupole and shielding interactions. These fluctuate randomly in the presence of molecular motion and may stimulate the relaxation of the system [24,25]. The relaxation of the rank-one dipole and rank-three octupole alignments is described for spin $I = \frac{3}{2}$ nuclei by the system

$$\frac{\partial}{\partial t}\begin{bmatrix}\tilde{\rho}_z(\xi_r,t)\\ \tilde{\rho}_{z^3}(\xi_r,t)\end{bmatrix} = \begin{bmatrix}\Delta_{z,z}(\xi_r,t) & \Delta_{z,z^3}(\xi_r,t)\\ \Delta_{z^3,z}(\xi_r,t) & \Delta_{z^3,z^3}(\xi_r,t)\end{bmatrix}\begin{bmatrix}\tilde{\rho}_z(\xi_r,t)\\ \tilde{\rho}_{z^3}(\xi_r,t)\end{bmatrix}, \tag{75}$$

while the relaxation of the rank-two quadrupole alignment obeys the equation

$$\frac{\partial}{\partial t}\tilde{\rho}_{z^2}(\xi_r,t) = \Delta_{z^2,z^2}(\xi_r,t)\tilde{\rho}_{z^2}(\xi_r,t), \tag{76}$$

where the elements $\Delta_{mn}(\xi_r,t) = \Delta^{Q}_{mn}(\xi_r,t) + \Delta^{S}_{mn}(\xi_r,t)$ of the relaxation operator are listed in Tables 4 and 5 in terms of the corresponding spectral densities. The equilibrium state of any nucleus at high fields is dominated by the rank-one dipole alignment. This state is transferred by any selective inversion pulse into rank-one dipole and rank-three octupole alignments. These odd-rank multipole alignments evolve simultaneously according to the above equations implying that the relaxation measured in inversion-recovery experiments cannot be exponential. This result has largely been ignored in the literature where most investigations have focused on systems with vanishing rank-three octupole alignments. These include solids with small quadrupole interactions and isotropic liquids and solutions [22]. However, the equations reveal that the relaxation of the rank-two quadrupole alignment may be exponential in the fast motion regime. It is difficult to excite this state in selective experiments and the relaxation of the rank-two quadrupole alignment is most easily measured in nonselective experiments on systems with small quadrupole interactions. This measurement provides an additional constraint that makes it possible to determine the spectral densities.

Table 5
Matrix elements of the spin $I = \frac{3}{2}$ shielding relaxation operator

$$\Delta^{S}_{z,z}(\xi_r,t) = \tfrac{1}{4}\omega_0^2\Big[J^{S}_{x,x}(\omega_0,t) + J^{S}_{y,y}(\omega_0,t) - \tfrac{36}{25}[J^{S}_{xz,xz}(\omega_0,t) + J^{S}_{yz,yz}(\omega_0,t)]\Big]$$

$$\Delta^{S}_{z^2,z^2}(\xi_r,t) = \tfrac{3}{4}\omega_0^2\Big[J^{S}_{x,x}(\omega_0,t) + J^{S}_{y,y}(\omega_0,t) - \tfrac{36}{25}[J^{S}_{xz,xz}(\omega_0,t) + J^{S}_{yz,yz}(\omega_0,t)]\Big]$$

$$\Delta^{S}_{z^3,z^3}(\xi_r,t) = \tfrac{3}{2}\omega_0^2\Big[J^{S}_{x,x}(\omega_0,t) + J^{S}_{y,y}(\omega_0,t) - \tfrac{36}{25}[J^{S}_{xz,xz}(\omega_0,t) + J^{S}_{yz,yz}(\omega_0,t)]\Big]$$

2.2.2. Relaxation of spin $I = \frac{5}{2}$ multipole alignments

The quadrupole and shielding relaxation of the three odd-rank multipole alignments of spin $I = \frac{5}{2}$ nuclei may be described by the system of simultaneous equations

Table 6
Matrix elements of the spin $I = \frac{5}{2}$ quadrupole relaxation operator

$$\Delta^{Q}_{z,z}(\xi_r,t) = -\tfrac{128}{25}[J^{Q}_{xz,xz}(\omega_0,t) + J^{Q}_{yz,yz}(\omega_0,t) + 4J^{Q}_{x^2-y^2,x^2-y^2}(2\omega_0,t) + 4J^{Q}_{xy,xy}(2\omega_0,t)]$$

$$\Delta^{Q}_{z,z^3}(\xi_r,t) = -\tfrac{1152}{25\sqrt{14}}[J^{Q}_{xz,xz}(\omega_0,t) + J^{Q}_{yz,yz}(\omega_0,t) - J^{Q}_{x^2-y^2,x^2-y^2}(2\omega_0,t) - J^{Q}_{xy,xy}(2\omega_0,t)]$$

$$\Delta^{Q}_{z^3,z}(\xi_r,t) = -\tfrac{1152}{25\sqrt{14}}[J^{Q}_{xz,xz}(\omega_0,t) + J^{Q}_{yz,yz}(\omega_0,t) - J^{Q}_{x^2-y^2,x^2-y^2}(2\omega_0,t) - J^{Q}_{xy,xy}(2\omega_0,t)]$$

$$\Delta^{Q}_{z^3,z^3}(\xi_r,t) = -\tfrac{16}{25}[82J^{Q}_{xz,xz}(\omega_0,t) + 82J^{Q}_{yz,yz}(\omega_0,t) + 83J^{Q}_{x^2-y^2,x^2-y^2}(2\omega_0,t) + 83J^{Q}_{xy,xy}(2\omega_0,t)]$$

$$\Delta^{Q}_{z^3,z^5}(\xi_r,t) = -\tfrac{32\sqrt{5}}{\sqrt{7}}[J^{Q}_{xz,xz}(\omega_0,t) + J^{Q}_{yz,yz}(\omega_0,t) - J^{Q}_{x^2-y^2,x^2-y^2}(2\omega_0,t) - J^{Q}_{xy,xy}(2\omega_0,t)]$$

$$\Delta^{Q}_{z^5,z^3}(\xi_r,t) = -\tfrac{32\sqrt{5}}{\sqrt{7}}[J^{Q}_{xz,xz}(\omega_0,t) + J^{Q}_{yz,yz}(\omega_0,t) - J^{Q}_{x^2-y^2,x^2-y^2}(2\omega_0,t) - J^{Q}_{xy,xy}(2\omega_0,t)]$$

$$\Delta^{Q}_{z^5,z^5}(\xi_r,t) = -16[2J^{Q}_{xz,xz}(\omega_0,t) + 2J^{Q}_{yz,yz}(\omega_0,t) + J^{Q}_{x^2-y^2,x^2-y^2}(2\omega_0,t) + J^{Q}_{xy,xy}(2\omega_0,t)]$$

$$\Delta^{Q}_{z^2,z^2}(\xi_r,t) = -\tfrac{48}{35}[22J^{Q}_{xz,xz}(\omega_0,t) + 22J^{Q}_{yz,yz}(\omega_0,t) + 27J^{Q}_{x^2-y^2,x^2-y^2}(2\omega_0,t) + 27J^{Q}_{xy,xy}(2\omega_0,t)]$$

$$\Delta^{Q}_{z^2,z^4}(\xi_r,t) = -\tfrac{96\sqrt{3}}{7}[J^{Q}_{xz,xz}(\omega_0,t) + J^{Q}_{yz,yz}(\omega_0,t) - J^{Q}_{x^2-y^2,x^2-y^2}(2\omega_0,t) - J^{Q}_{xy,xy}(2\omega_0,t)]$$

$$\Delta^{Q}_{z^4,z^2}(\xi_r,t) = -\tfrac{96\sqrt{3}}{7}[J^{Q}_{xz,xz}(\omega_0,t) + J^{Q}_{yz,yz}(\omega_0,t) - J^{Q}_{x^2-y^2,x^2-y^2}(2\omega_0,t) - J^{Q}_{xy,xy}(2\omega_0,t)]$$

$$\Delta^{Q}_{z^4,z^4}(\xi_r,t) = -\tfrac{16}{7}[26J^{Q}_{xz,xz}(\omega_0,t) + 26J^{Q}_{yz,yz}(\omega_0,t) + 23J^{Q}_{x^2-y^2,x^2-y^2}(2\omega_0,t) + 23J^{Q}_{xy,xy}(2\omega_0,t)]$$

$$\frac{\partial}{\partial t}\begin{bmatrix}\tilde{\rho}_z(\xi_r,t)\\ \tilde{\rho}_{z^3}(\xi_r,t)\\ \tilde{\rho}_{z^5}(\xi_r,t)\end{bmatrix} = \begin{bmatrix}\Delta_{z,z}(\xi_r,t) & \Delta_{z,z^3}(\xi_r,t) & 0\\ \Delta_{z^3,z}(\xi_r,t) & \Delta_{z^3,z^3}(\xi_r,t) & \Delta_{z^3,z^5}(\xi_r,t)\\ 0 & \Delta_{z^5,z^3}(\xi_r,t) & \Delta_{z^5,z^5}(\xi_r,t)\end{bmatrix} \times \begin{bmatrix}\tilde{\rho}_z(\xi_r,t)\\ \tilde{\rho}_{z^3}(\xi_r,t)\\ \tilde{\rho}_{z^5}(\xi_r,t)\end{bmatrix}, \tag{77}$$

whereas the relaxation of the two even-rank multipole alignments is defined by

$$\frac{\partial}{\partial t}\begin{bmatrix}\tilde{\rho}_{z^2}(\xi_r,t)\\ \tilde{\rho}_{z^4}(\xi_r,t)\end{bmatrix} = \begin{bmatrix}\Delta_{z^2,z^2}(\xi_r,t) & \Delta_{z^2,z^4}(\xi_r,t)\\ \Delta_{z^4,z^2}(\xi_r,t) & \Delta_{z^4,z^4}(\xi_r,t)\end{bmatrix}\begin{bmatrix}\tilde{\rho}_{z^2}(\xi_r,t)\\ \tilde{\rho}_{z^4}(\xi_r,t)\end{bmatrix}, \tag{78}$$

where the elements of the relaxation operator are listed in Tables 6 and 7 in terms of the corresponding spectral densities. The equilibrium state of predominantly rank-one dipole alignment is distributed by any selective inversion pulse among rank-one dipole, rank-three octupole, and rank-five multipole alignments. The simultaneous evolution of these alignments implies that the relaxation cannot be described by simple exponentials and relaxation times. Although it is useful to measure the relaxation of the even-rank multipole alignments these states are difficult or impossible to create in selective experiments. Because the even-rank multipole alignments evolve simultaneously the relaxation of these states cannot be exponential.

Table 7
Matrix elements of the spin $I = \frac{5}{2}$ shielding relaxation operator

$$\Delta^{S}_{z,z}(\xi_r,t) = \tfrac{1}{4}\omega_0^2\left[J^{S}_{x,x}(\omega_0,t) + J^{S}_{y,y}(\omega_0,t) - \tfrac{256}{25}[J^{S}_{xz,xz}(\omega_0,t) + J^{S}_{yz,yz}(\omega_0,t)]\right]$$

$$\Delta^{S}_{z^2,z^2}(\xi_r,t) = \tfrac{3}{4}\omega_0^2\left[J^{S}_{x,x}(\omega_0,t) + J^{S}_{y,y}(\omega_0,t) - \tfrac{256}{25}[J^{S}_{xz,xz}(\omega_0,t) + J^{S}_{yz,yz}(\omega_0,t)]\right]$$

$$\Delta^{S}_{z^3,z^3}(\xi_r,t) = \tfrac{3}{2}\omega_0^2\left[J^{S}_{x,x}(\omega_0,t) + J^{S}_{y,y}(\omega_0,t) - \tfrac{256}{25}[J^{S}_{xz,xz}(\omega_0,t) + J^{S}_{yz,yz}(\omega_0,t)]\right]$$

$$\Delta^{S}_{z^4,z^4}(\xi_r,t) = \tfrac{5}{2}\omega_0^2\left[J^{S}_{x,x}(\omega_0,t) + J^{S}_{y,y}(\omega_0,t) - \tfrac{256}{25}[J^{S}_{xz,xz}(\omega_0,t) + J^{S}_{yz,yz}(\omega_0,t)]\right]$$

$$\Delta^{S}_{z^5,z^5}(\xi_r,t) = \tfrac{15}{4}\omega_0^2\left[J^{S}_{x,x}(\omega_0,t) + J^{S}_{y,y}(\omega_0,t) - \tfrac{256}{25}[J^{S}_{xz,xz}(\omega_0,t) + J^{S}_{yz,yz}(\omega_0,t)]\right]$$

2.2.3. Effects of relaxation anisotropy on partially relaxed lineshapes

It is instructive to investigate in more detail the effects of anisotropic motion and relaxation on solid-state central transition NMR spectra of some representative model systems involving half-integer quadrupole nuclei. This will not only demonstrate the potential of the methods introduced in this paper but also provide some guidelines that may be useful in implementing the experiments and interpreting the results. It is known that many systems involving half-integer quadrupole nuclei have considerable quadrupole interactions. This makes it impossible to observe the satellite transitions and the experiments are usually designed to record the central transition selectively [37–39]. Because the central transition is dominated by the second-order quadrupole and first-order shielding interactions the spectra have characteristic lineshapes that may provide information about

the structural and motional details of the system. As we have already discussed it is essential for any accurate investigation of molecular motion to record both fully and partially relaxed lineshapes. The influence of molecular motion on fully relaxed central transition NMR spectra has previously been discussed and shown to be useful to characterize systems in the intermediate motion regime [40–42]. In the case of strong quadrupole interactions the fully relaxed lineshapes are most easily obtained using the central transition spin-echo experiment while the partially relaxed spectra may be recorded by implementing the central transition inversion-recovery experiment. The pulse sequences used in these experiments are illustrated in Fig. 1 which also includes diagrams of the allowed coherence transfer pathways. It is noted that the pulse sequences may be applied to any half-integer quadrupole nucleus and any solid material.

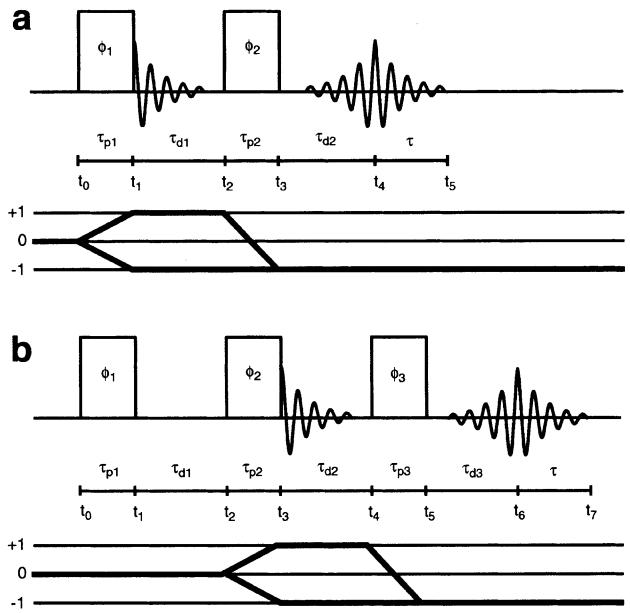

Fig. 1. Experimental schemes used for central transition NMR spectroscopy of half-integer quadrupole nuclei. The central transition spin-echo experiment (a) is implemented to obtain fully relaxed spectra. The sequence has two selective rf pulses of lengths τ_{p1} and τ_{p2} and phases φ_{p1} and φ_{p2} and two delay periods of lengths τ_{d1} and τ_{d2}. The first rf pulse creates single-quantum coherences that relax during the first delay period. The sensitivity is optimized by adjusting the pulse length so that $\tau_{p1}\omega_{eff} = \frac{\pi}{2}$ where the effective rf field strength $\omega_{eff} = \omega_{rf}[I + \frac{1}{2}]$ for the central transition. The second rf pulse refocuses the single-quantum coherences and creates an echo at the end of the second delay period. The refocusing is optimized for the central transition by matching the pulse length so that $\tau_{p2}\omega_{eff} = \pi$. The central transition inversion-recovery experiment (b) is used to obtain partially relaxed lineshapes. The sequence has a selective rf pulse of length τ_{p1} and phase φ_{p1} to invert the central transition. For optimum inversion the pulse length is adjusted so that $\tau_{p1}\omega_{eff} = \pi$. The inversion creates multipole alignments that relax during the first delay period of length τ_{d1} before being monitored by the central transition spin-echo sequence. This has two selective rf pulses of lengths τ_{p2} and τ_{p3} and phases φ_{p2} and φ_{p3} and two delay periods of lengths τ_{d2} and τ_{d3}.

The density operator formalism introduced in the preceding sections has formed the basis for the development of Fortran 95 programs to simulate both fully and partially relaxed lineshapes for any half-integer quadrupole nucleus. These programs include all multipole coherences and alignments and may be applied to simulate both satellite and central transition spectra. Although the density operator formalism makes simulations of molecular motion much more difficult it is the most efficient approach to calculate coherence transfer processes during periods of rf irradiation and represent effects of finite rf pulse length. The simulation of finite rf pulse length effects is very difficult in the presence of molecular motion and has previously only been accomplished for deuterons [33]. In selective experiments implementing weak rf fields the effects of finite pulse length may be pronounced and cannot usually be ignored for half-integer quadrupole nuclei. This is demonstrated in Fig. 2 where we show simulations of central transition lineshapes for both nonselective and selective experiments. The effects of finite pulse length are vanishing in nonselective experiments where the quadrupole and shielding interactions may be ignored during short periods of strong rf irradiation. However, because of the stringent rf requirements it is impossible to implement nonselective experiments for systems with large quadrupole and shielding interactions. In these cases the systems may be studied by observing the central transition in selective experiments using weak rf fields and long pulses. For most half-integer quadrupole nuclei the quadrupole and shielding interactions are substantial and must be included in the course of selective rf irra-

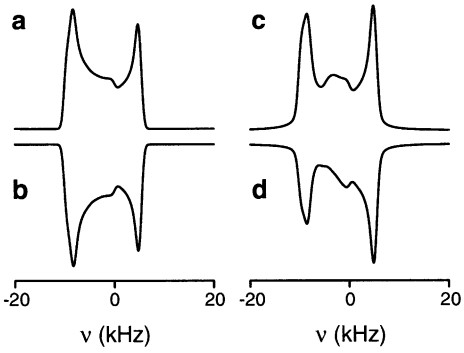

Fig. 2. Simulated central transition inversion-recovery ^{17}O NMR spectra of a polycrystalline sample demonstrating the effects of nonselective (a,b) and selective (c,d) excitation. The results include fully relaxed (a,c) and fully inverted (b,d) spectra for ultraslow molecular motion. The calculations used the Larmor frequency $\nu_0 = 54.24\,MHz$, quadrupole coupling constant $C_Q = 5.0\,MHz$, and quadrupole asymmetry parameter $\eta_Q = 0.10$. In these simulations nonselective excitation corresponds to infinitely strong and short rf pulses while selective excitation is defined by the rf field strength $\nu_{rf} = 25\,kHz$, pulse lengths $\tau_{p1} = \frac{20}{3}\,\mu s$, $\tau_{p2} = \frac{10}{3}\,\mu s$, and $\tau_{p3} = \frac{20}{3}\,\mu s$, and delay length $\tau_{d2} = 50\,\mu s$. The effects of finite rf pulse length are evident by comparing the spectra for nonselective and selective excitation.

diation. The central transition is usually very broad making uniform selective excitation and inversion impossible. The result is that the lineshapes exhibit significant phase and intensity distortions. The phase distortions may usually be corrected by shifting the echo maximum. However, the intensity distortions cannot be eliminated and must be simulated by explicit calculation. The results presented in Fig. 2 show that it is impossible to accurately simulate central transition lineshapes without including the effects of finite rf pulse length. It is obvious that the values of the quadrupole and shielding parameters may become inaccurate if the intensity distortion effects are ignored in the simulations. Moreover, it is impossible to accurately characterize the motion without considering the effects of finite rf pulse length. The only experimental procedures to reduce the distortion effects involve using composite pulses or reducing the pulse lengths. Because these techniques may reduce the sensitivity and introduce other distortions it is usually better to include the effects of finite pulse length in the calculations. It is obvious that the lineshapes may exhibit additional intensity distortions in the case of imperfect powders with a nonuniform distribution of crystallites. These distortions can only be simulated if the crystallite distribution is known which is usually not the case for most systems. The best experimental procedure to eliminate these distortions is to ensure that the experiments are performed on finely ground powders.

As an example we have calculated central transition spin-echo and inversion-recovery ^{17}O NMR spectra for an oxygen nucleus reorienting between three different motional states. These states are illustrated in Fig. 3 and correspond to three different orientations of the principal axis system of the quadrupole tensor relative to the crystallite fixed axis system. Because the lineshapes depend strongly on the precise geometry this system is useful for studying the influence of different tensor orientations and rate constants. The effects of anisotropic molecular motion on fully relaxed lineshapes are demonstrated in Fig. 4 which shows the calculated central transition spin-echo ^{17}O NMR spectra for two different sets of tensor orientations. It is seen that there are no distinct differences between the spectra in the slow motion regime ($k_{mn} \leqslant 10^3$ Hz) making it almost impossible to differentiate between different tensor orientations and determine the rate constants. The results are more interesting in the intermediate motion regime (10^3 Hz $\leqslant k_{mn} \leqslant 10^6$ Hz) where it is possible to measure the tensor orientations and rate constants with relatively high accuracy. However, it is important to realize that it is difficult or impossible to distinguish small differences in the tensor orientations and rate constants and that there may be several different models that produce the same fully relaxed lineshapes. In the fast motion regime

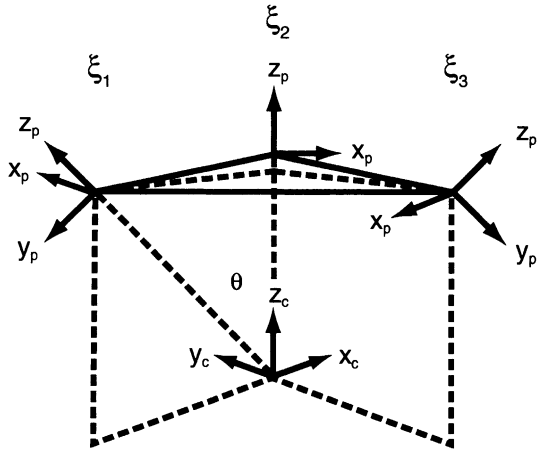

Fig. 3. Geometry of threefold rotation showing the orientations $\mathbf{\Omega}_2(\xi_k) = \{\frac{3\pi}{2}, \theta, \frac{2\pi[k-1]}{3}\}$ of the principal axis system of the quadrupole tensor relative to the crystallite fixed axis system.

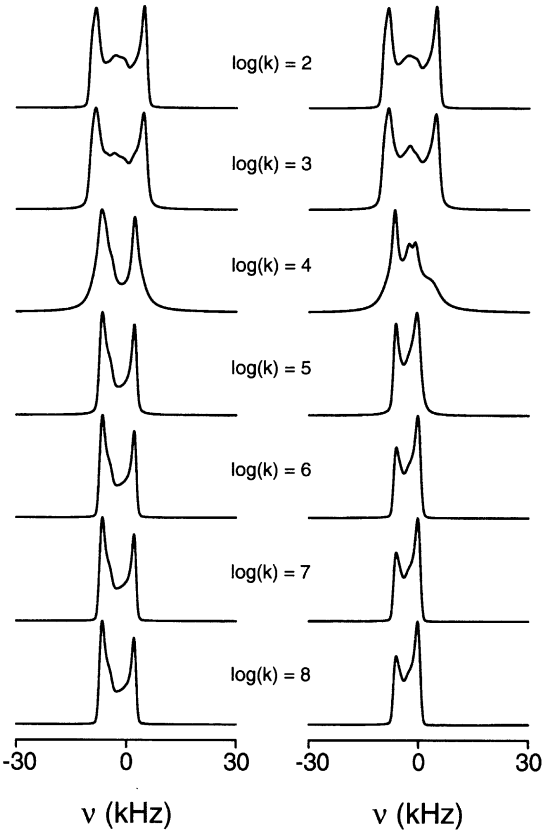

Fig. 4. Simulated central transition spin-echo ^{17}O NMR spectra of a polycrystalline sample as function of the rate constant k for reorientation between three different orientations $\mathbf{\Omega}_2(\xi_k) = \{\frac{3\pi}{2}, \frac{\pi}{9}, \frac{2\pi[k-1]}{3}\}$ (left column) and $\mathbf{\Omega}_2(\xi_k) = \{\frac{3\pi}{2}, \frac{\pi}{6}, \frac{2\pi[k-1]}{3}\}$ (right column) of the principal axis system of the quadrupole tensor. The calculations used the Larmor frequency $\nu_0 = 54.24$ MHz, rf field strength $\nu_{rf} = 25$ kHz, pulse lengths $\tau_{p1} = \frac{10}{3}$ μs and $\tau_{p2} = \frac{20}{3}$ μs, delay length $\tau_{d1} = 50$ μs, quadrupole coupling constant $C_Q = 5.0$ MHz, and quadrupole asymmetry parameter $\eta_Q = 0.10$. The effects of finite rf pulse length have been included in the simulations.

($k_{mn} \geqslant 10^6$ Hz) the spectra gradually converge to an invariant lineshape defined by the motionally averaged Hamiltonian. For central transition spectra dominated by the second-order quadrupole interaction this lineshape cannot be described by simple average quadrupole parameters but must be calculated explicitly for any given system [40]. The results indicate that it is possible to differentiate between different tensor orientations. However, there are usually many different models that give the same averaged lineshapes, making the interpretation of the results difficult or ambiguous. Moreover, because the spectra become invariant it is impossible to determine the rate constants in the fast motion regime. In many cases the only result that can be obtained is a lower limit on the rate constants. These results show that fully relaxed lineshapes obtained using the central transition spin-echo experiment are very useful in the intermediate motion regime but may lead to inaccurate or ambiguous results in the slow and fast motion regimes.

It is known that the properties of many important solid materials are determined by either slow or fast anisotropic molecular motion. Although the motion may be temperature activated it is not always possible to study these systems in the intermediate motion regime where the spectra are more easily interpreted. The problem is especially difficult for temperature sensitive materials and systems where the structure and motion may change as a result of phase transitions. In order to resolve any potential ambiguity and inaccuracy in characterizing the motion it is useful to investigate the partially relaxed lineshapes. The most eminent advantages of studying partially relaxed spectra are that the accuracy of the results is improved significantly and the number of possible motional models is reduced. As an example we have calculated the partially relaxed spectra corresponding to the system described above involving three motional states.

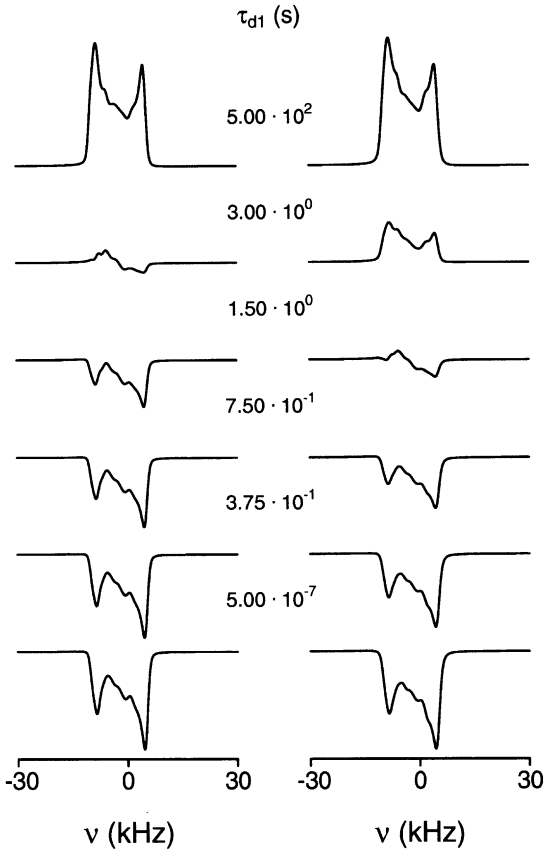

Fig. 5. Simulated central transition inversion-recovery ^{17}O NMR spectra of a polycrystalline sample as function of the length τ_{d1} of the relaxation delay. The motion has the rate constant $\log(k) = 3.00$ (left column) and $\log(k) = 3.25$ (right column) and involves transitions between three equally probable orientations $\mathbf{\Omega}_2(\xi_k) = \{\frac{3\pi}{2}, \frac{\pi}{9}, \frac{2\pi[k-1]}{3}\}$ of the principal axis system of the quadrupole tensor. The calculations implemented the Larmor frequency $\nu_0 = 54.24$ MHz, rf field strength $\nu_{rf} = 25$ kHz, pulse lengths $\tau_{p1} = \frac{20}{3}\mu$s, $\tau_{p2} = \frac{10}{3}\mu$s, and $\tau_{p3} = \frac{20}{3}\mu$s, delay length $\tau_{d2} = 50\,\mu$s, quadrupole coupling constant $C_Q = 5.0$ MHz, and quadrupole asymmetry parameter $\eta_Q = 0.10$. The simulations include effects of finite rf pulse length.

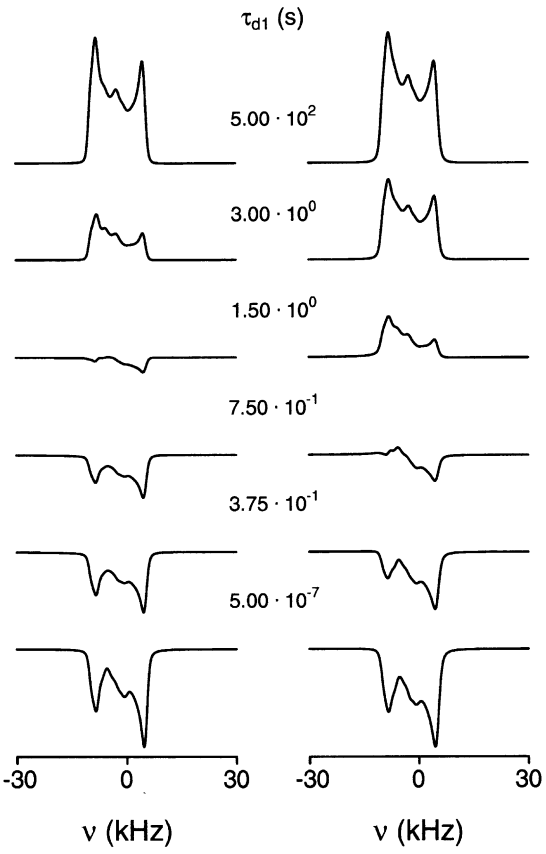

Fig. 6. Simulated central transition inversion-recovery ^{17}O NMR spectra of a polycrystalline sample as function of the length τ_{d1} of the relaxation delay. The motion is specified by the rate constant $\log(k) = 3.00$ (left column) and $\log(k) = 3.25$ (right column) and involves reorientation between three different orientations $\mathbf{\Omega}_2(\xi_k) = \{\frac{3\pi}{2}, \frac{\pi}{6}, \frac{2\pi[k-1]}{3}\}$ of the principal axis system of the quadrupole tensor.

The results for slow molecular motion are shown in Figs. 5–8 where we compare central transition inversion-recovery ^{17}O NMR spectra for some representative models that differ only slightly in the tensor orientations and rate constants. For these models it is seen that the fully relaxed lineshapes are almost independent of the tensor orientations and rate constants, making it difficult or impossible to characterize the motion accurately and unambiguously. However, it is evident that the partially relaxed lineshapes are very sensitive to the values of the rate constants and tensor orientations. The differences between the models are most pronounced for the spectra near the inversion point where the intensities change from negative to positive. This is also the point where the relaxation anisotropy is expressed most strongly. The relaxation anisotropy is readily identified by noting that the spectral components at lower frequencies relax much faster than those at higher frequencies. The origin of the relaxation anisotropy may be understood by examining the form of the spectral densities (Eq. (42)). Because these involve the elements of the anisotropic Hamiltonian they depend explicitly on the crystallite orientation. The result is that the relaxation rate becomes a function of the orientation and is different for each crystallite. The anisotropy of the Hamiltonian implies that each crystallite orientation defines a spectral component at the corresponding central transition frequency. In the case of a polycrystalline powder the lineshape is a superposition of spectral components defined by all possible crystallite orientations. Because the relaxation rate for each individual spectral component is different the relaxation of the powder lineshape may exhibit a strong anisotropy.

The calculations presented in Figs. 5–8 demonstrate that relaxation measurements make it possible to distinguish very small differences in the rate constants and tensor orientations. For any given set of tensor orientations the spectra are seen to have similar relaxation anisotropies. However, the models may easily be differentiated because the system with the largest rate constants relaxes significantly faster. Similarly, because different tensor orientations lead to different relaxation anisotropies and relaxation rates it is possible to

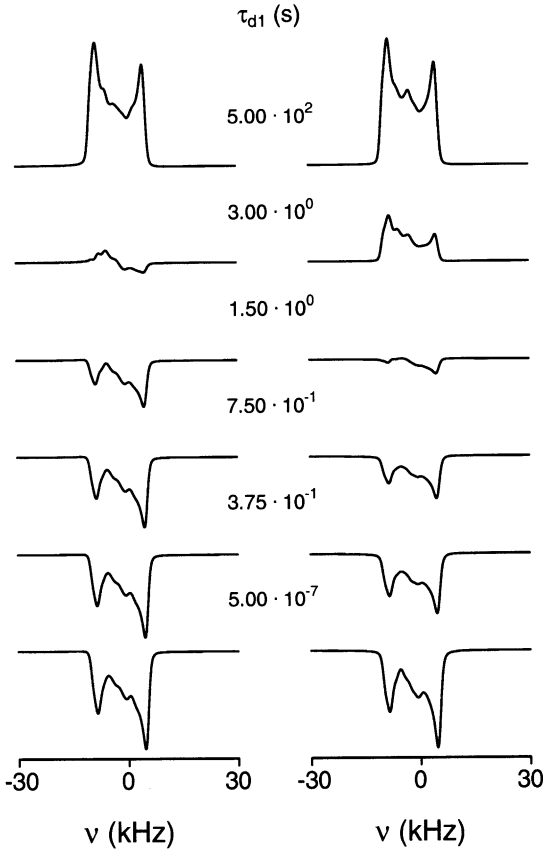

Fig. 7. Simulated central transition inversion-recovery ^{17}O NMR spectra of a polycrystalline sample as function of the length τ_{d1} of the relaxation delay. The motion has the rate constant $\log(k) = 3.00$ and involves transitions between three equally probable orientations $\mathbf{\Omega}_2(\xi_k) = \{\frac{3\pi}{2}, \frac{\pi}{9}, \frac{2\pi[k-1]}{3}\}$ (left column) and $\mathbf{\Omega}_2(\xi_k) = \{\frac{3\pi}{2}, \frac{\pi}{6}, \frac{2\pi[k-1]}{3}\}$ (right column) of the principal axis system of the quadrupole tensor.

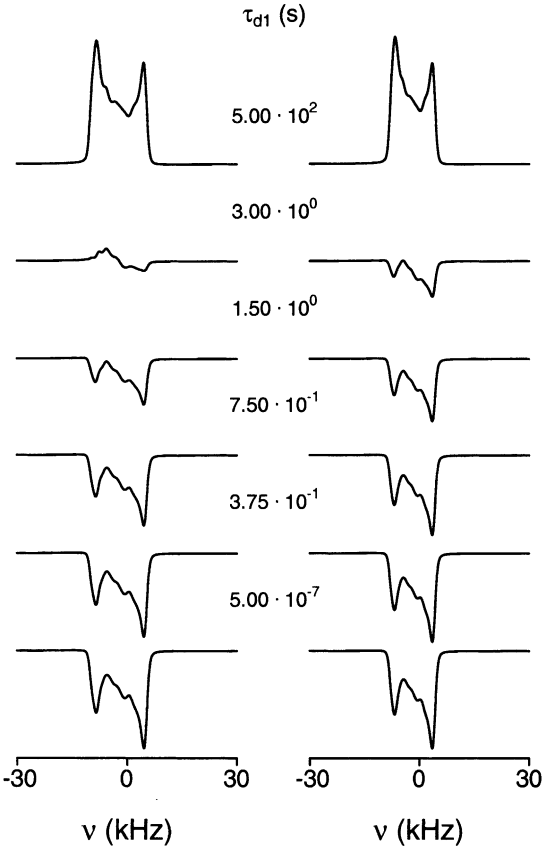

Fig. 8. Simulated central transition inversion-recovery ^{17}O NMR spectra of a polycrystalline sample as function of the length τ_{d1} of the relaxation delay. The motion has the rate constant $\log(k) = 3.00$ and involves reorientation between three different orientations $\mathbf{\Omega}_2(\xi_k) = \{\frac{3\pi}{2}, \frac{\pi}{9}, \frac{2\pi[k-1]}{3}\}$ of the principal axis system of the quadrupole tensor. The calculations implemented the Larmor frequency $\nu_0 = 54.24\,\text{MHz}$ (left column) and $\nu_0 = 67.80\,\text{MHz}$ (right column).

distinguish between different geometries. The results are most easily understood by considering the form of the spectral densities (Eq. (42)). By extending the upper limit on the integral to infinity one finds that

$$J_{p_1p_2}(n\omega_0) = -2\sum_{k=1}^{N}\sum_{l=1}^{N}\sum_{m=1}^{N} H_{1p_1}(\xi_l)H_{1p_2}(\xi_k)b_{kl}^{(m)} \times \frac{\lambda_m}{\lambda_m^2 + n^2\omega_0^2}, \tag{79}$$

which depends on the eigenvalues λ_m of the stochastic matrix and the frequency $n\omega_0$ of the particular nuclear spin transition. This result is strictly valid only for fast molecular motion where the spectral densities become time independent [22–25]. However, it represents an approximation that is useful to discuss the form of the spectral densities. Because the elements of the relaxation operator depend on the spectral densities it is evident that these provide a measure of the relaxation rates. The different motional regimes may be distinguished by noting that the eigenvalues of the stochastic matrix are all real and negative and of the order of the rate constants. In the case of slow and intermediate molecular motion ($|\lambda_m| \ll \omega_0$) the spectral densities may be approximated by

$$J_{p_1p_2}(n\omega_0) = -2\sum_{k=1}^{N}\sum_{l=1}^{N}\sum_{m=1}^{N} H_{1p_1}(\xi_l)H_{1p_2}(\xi_k)b_{kl}^{(m)}\frac{\lambda_m}{n^2\omega_0^2}, \tag{80}$$

which reveal that the corresponding relaxation rate is relatively small. However, the relaxation rate is an increasing function of the rate constants. In the case of quadrupole relaxation the relaxation rate is a decreasing function of the Larmor frequency. This frequency dependence is shown in Fig. 8 where the lineshapes are presented for two different Larmor frequencies. It is seen that the system with the highest Larmor frequency relaxes slower. Because the shielding Hamiltonian is proportional to the Larmor frequency there is no frequency dependence for a system dominated by shielding relaxation.

In the case of fast molecular motion the calculated central transition inversion-recovery ^{17}O NMR spectra

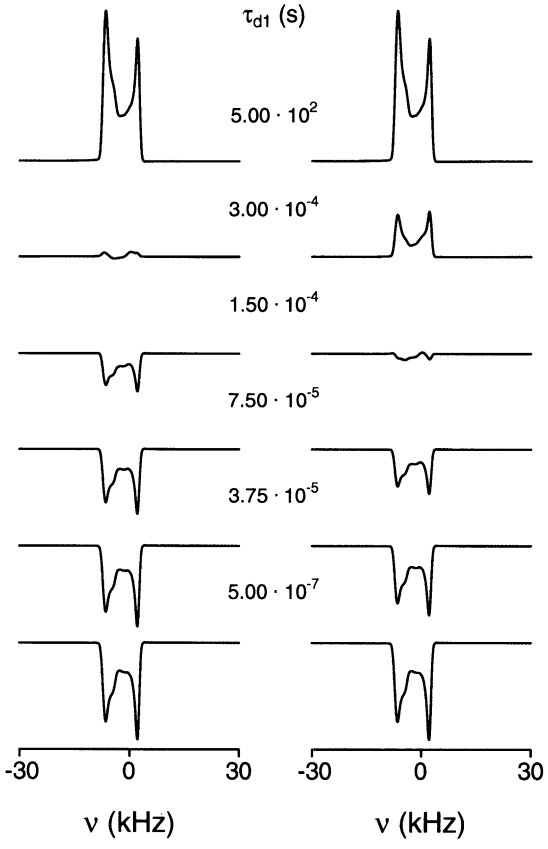

Fig. 9. Simulated central transition inversion-recovery ^{17}O NMR spectra of a polycrystalline sample as function of the length τ_{d1} of the relaxation delay. The motion is characterized by the rate constant $\log(k) = 7.00$ (left column) and $\log(k) = 7.25$ (right column) and involves transitions between three different orientations $\mathbf{\Omega}_2(\xi_k) = \{\frac{3\pi}{2}, \frac{\pi}{9}, \frac{2\pi[k-1]}{3}\}$ of the principal axis system of the quadrupole tensor.

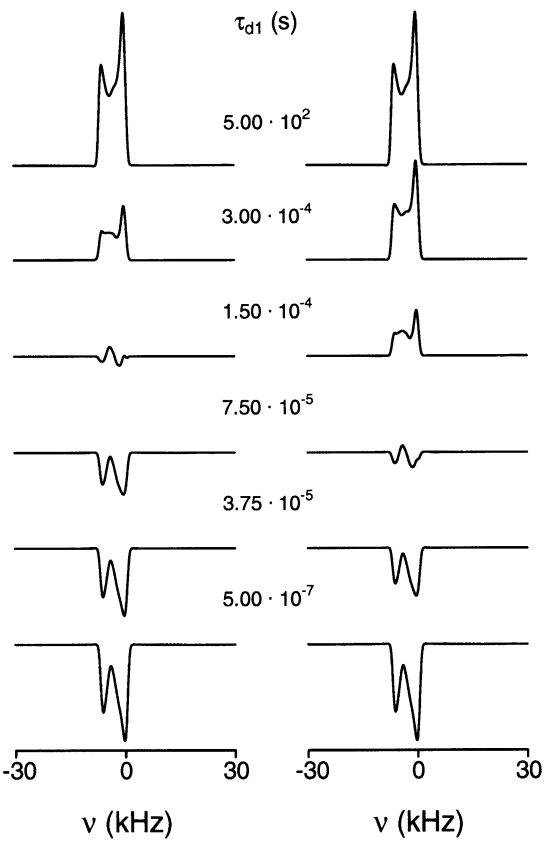

Fig. 10. Simulated central transition inversion-recovery ^{17}O NMR spectra of a polycrystalline sample as function of the length τ_{d1} of the relaxation delay. The motion has the rate constant $\log(k) = 7.00$ (left column) and $\log(k) = 7.25$ (right column) and involves reorientation between three equally probable orientations $\mathbf{\Omega}_2(\xi_k) = \{\frac{3\pi}{2}, \frac{\pi}{6}, \frac{2\pi[k-1]}{3}\}$ of the principal axis system of the quadrupole tensor.

are shown in Figs. 9–12 for the models described above involving three motional states. The most characteristic feature of the spectra in the fast motion regime is that the lineshapes are defined by a motionally averaged second-order quadrupole interaction. The lineshapes are relatively complicated and cannot be described in terms of average quadrupole parameters [40]. Although the spectra are seen to be sensitive to the tensor orientations and rate constants there are many different models that may reproduce the same fully relaxed lineshapes. This ambiguity may often be resolved by studying the partially relaxed lineshapes that are seen to be very sensitive to the precise tensor orientations and rate constants. For any given set of tensor orientations the spectra exhibit a similar relaxation anisotropy but the relaxation rate is different depending on the rate constants. Because the relaxation rate depends strongly on the rate constants it is possible to distinguish between models that differ only slightly. Similarly, for partially relaxed spectra calculated with the same rate constants there are distinct differences depending on the tensor orientations. It is

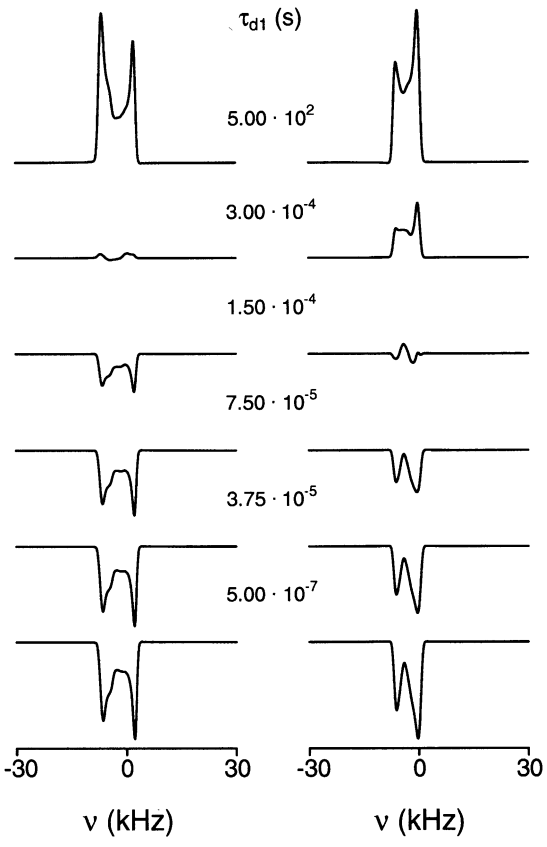

Fig. 11. Simulated central transition inversion-recovery ^{17}O NMR spectra of a polycrystalline sample as function of the length τ_{d1} of the relaxation delay. The motion has the rate constant $\log(k) = 7.00$ and involves transitions between three different orientations $\mathbf{\Omega}_2(\xi_k) = \{\frac{3\pi}{2}, \frac{\pi}{9}, \frac{2\pi[k-1]}{3}\}$ (left column) and $\mathbf{\Omega}_2(\xi_k) = \{\frac{3\pi}{2}, \frac{\pi}{6}, \frac{2\pi[k-1]}{3}\}$ (right column) of the principal axis system of the quadrupole tensor.

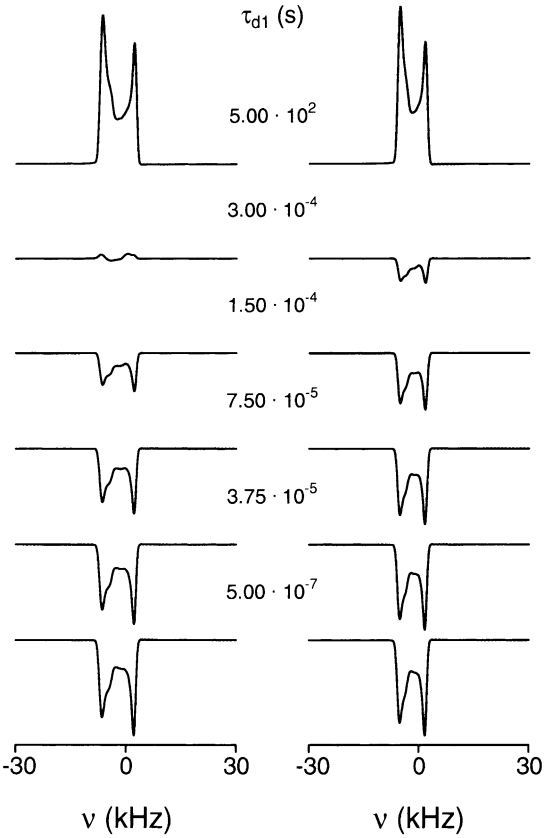

Fig. 12. Simulated central transition inversion-recovery ^{17}O NMR spectra of a polycrystalline sample as function of the length τ_{d1} of the relaxation delay. The motion has the rate constant $\log(k) = 7.00$ and involves reorientation between three equally probable orientations $\mathbf{\Omega}_2(\xi_k) = \{\frac{3\pi}{2}, \frac{\pi}{9}, \frac{2\pi[k-1]}{3}\}$ of the principal axis system of the quadrupole tensor. The calculations implemented the Larmor frequency $\nu_0 = 54.24\,\text{MHz}$ (left column) and $\nu_0 = 67.80\,\text{MHz}$ (right column).

seen that the relaxation rate varies considerably and may be very high in the fast motion regime.

The behavior of the relaxation rate is readily explained by considering the functional form of the spectral densities. As discussed above the spectral densities and corresponding relaxation rates are increasing functions of the rate constants provided that the motion is sufficiently slow. However, it is evident that the spectral densities have maximum intensity when $\lambda_m = n\omega_0$ and this intensity may be orders of magnitude higher than in the slow motion regime. The existence of the relaxation maximum is consistent with the fact that the relaxation is fastest when the oscillation frequencies of the local magnetic fields generated by the motion match the nuclear spin transition frequencies. In the case of either much faster or slower motion the spectral densities decrease significantly, making the relaxation of the system orders of magnitude slower. The results presented in Figs. 9–12 for the fast motion regime demonstrate that the relaxation rate is an increasing function of the rate constants and considerably higher compared with the slow motion regime. This shows that the relaxation rate

is close to but below its expected maximum. As discussed above the quadrupole relaxation rate depends explicitly on the Larmor frequency below the relaxation maximum. This is demonstrated in Fig. 12 where the partially relaxed spectra are compared for different Larmor frequencies. It is obvious that the frequency dependence may be useful for diagnostic purposes. The shielding relaxation is clearly independent of the Larmor frequency below the relaxation maximum.

The existence of a relaxation maximum suggests that the relaxation rate is a decreasing function of the rate constants for ultrafast molecular motion. This result is verified by considering the form of the spectral densities. In the case of ultrafast motion ($|\lambda_m| \gg \omega_0$) these may be approximated by

$$J_{p_1p_2}(n\omega_0) = -2\sum_{k=1}^{N}\sum_{l=1}^{N}\sum_{m=1}^{N} H_{1p_1}(\xi_l)H_{1p_2}(\xi_k)b_{kl}^{(m)}\lambda_m^{-1}, \tag{81}$$

which are decreasing functions of the rate constants. The equation demonstrates that the relaxation rate is independent of the Larmor frequency for the quadrupole interaction. However, in the case of the shielding interaction the relaxation rate becomes a quadratic function of the Larmor frequency. It is useful to compare the simulations discussed above for the fast motion regime with the calculations shown in Figs. 13–16 for ultrafast molecular motion. It is seen that the fully relaxed lineshapes are identical in the fast and ultrafast motion regimes. However, the quadrupole relaxation rate is not only smaller but also a decreasing function of the rate constants for ultrafast molecular motion. Moreover, the quadrupole relaxation rate is independent of the Larmor frequency. This is characteristic for quadrupole relaxation above the relaxation maximum and highly diagnostic of ultrafast molecular motion. The simulations reveal that the partially relaxed spectra in the fast and ultrafast motion regime are very sensitive to the values of the rate constants and tensor orientations. Moreover, by examining the frequency dependence of the relaxation rate it is possible to distinguish between motional regimes corresponding to fast and ultrafast motion where the lineshapes and relaxation rates may be similar.

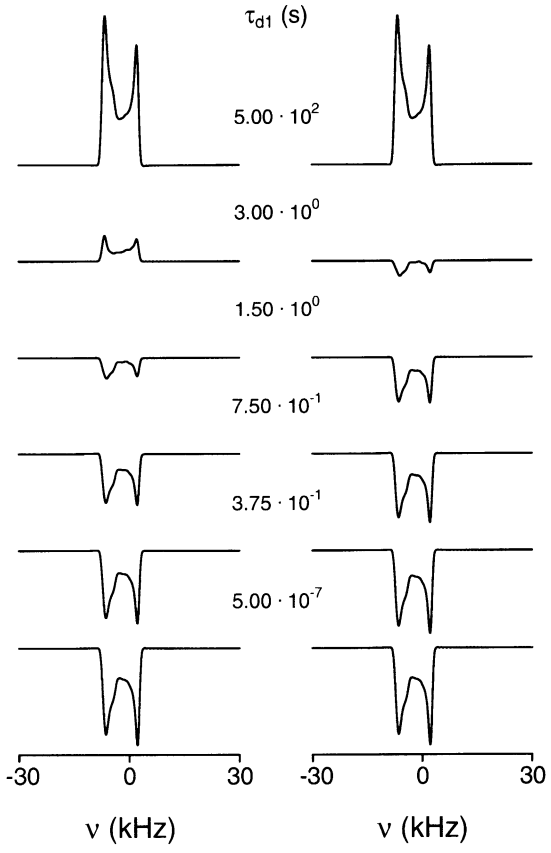

Fig. 13. Simulated central transition inversion-recovery ^{17}O NMR spectra of a polycrystalline sample as function of the length τ_{d1} of the relaxation delay. The motion is characterized by the rate constant $\log(k) = 13.00$ (left column) and $\log(k) = 13.25$ (right column) and involves transitions between three different orientations $\mathbf{\Omega}_2(\xi_k) = \{\frac{3\pi}{2}, \frac{\pi}{9}, \frac{2\pi[k-1]}{3}\}$ of the principal axis system of the quadrupole tensor.

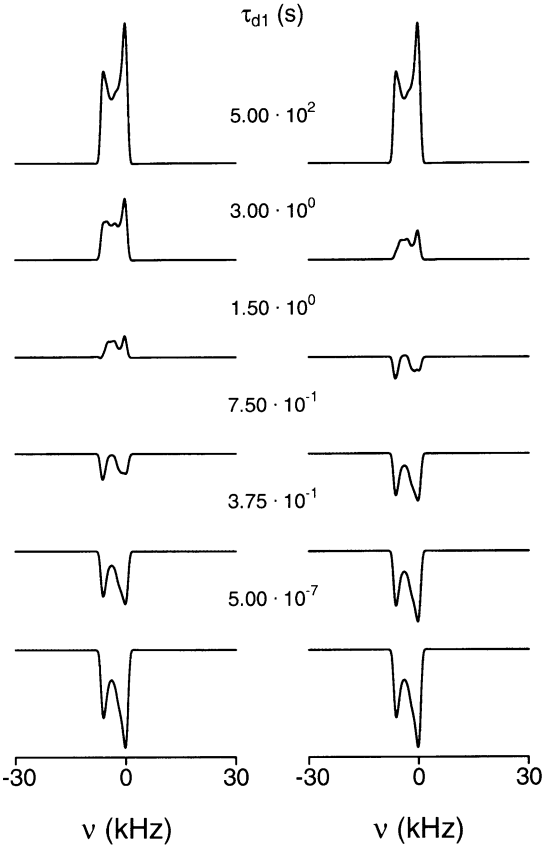

Fig. 14. Simulated central transition inversion-recovery ^{17}O NMR spectra of a polycrystalline sample as function of the length τ_{d1} of the relaxation delay. The motion has the rate constant $\log(k) = 13.00$ (left column) and $\log(k) = 13.25$ (right column) and involves reorientation between three different orientations $\mathbf{\Omega}_2(\xi_k) = \{\frac{3\pi}{2}, \frac{\pi}{6}, \frac{2\pi[k-1]}{3}\}$ of the principal axis system of the quadrupole tensor.

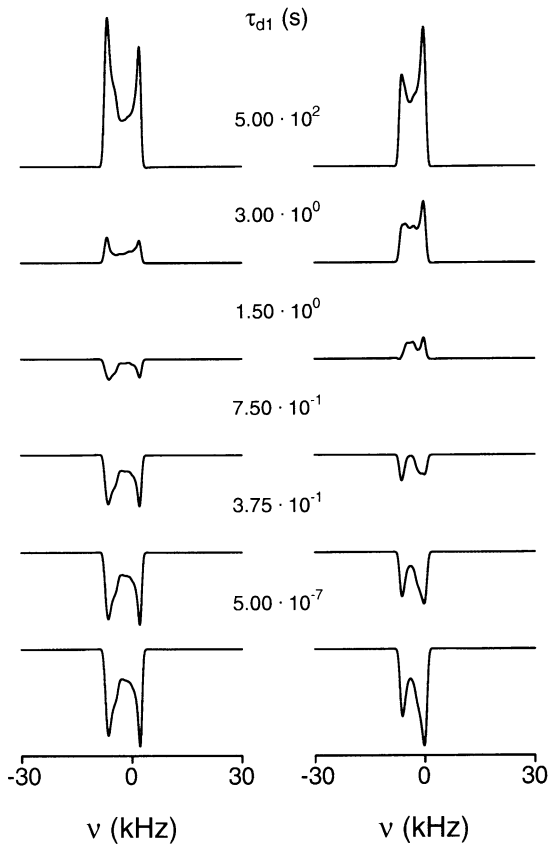

Fig. 15. Simulated central transition inversion-recovery ^{17}O NMR spectra of a polycrystalline sample as function of the length τ_{d1} of the relaxation delay. The motion has the rate constant $\log(k) = 13.00$ and involves transitions between three different orientations $\mathbf{\Omega}_2(\xi_k) = \{\frac{3\pi}{2}, \frac{\pi}{9}, \frac{2\pi[k-1]}{3}\}$ (left column) and $\mathbf{\Omega}_2(\xi_k) = \{\frac{3\pi}{2}, \frac{\pi}{6}, \frac{2\pi[k-1]}{3}\}$ (right column) of the principal axis system of the quadrupole tensor.

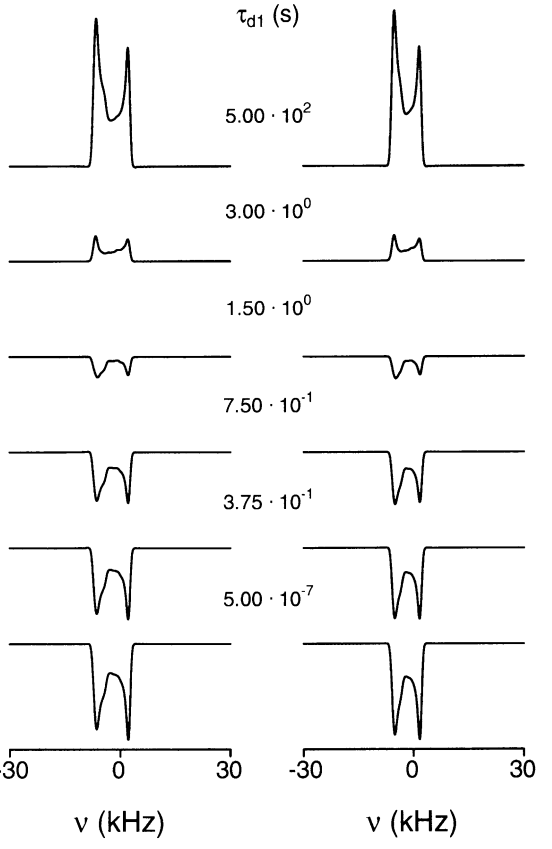

Fig. 16. Simulated central transition inversion-recovery ^{17}O NMR spectra of a polycrystalline sample as function of the length τ_{d1} of the relaxation delay. The motion has the rate constant $\log(k) = 13.00$ and involves reorientation between three different orientations $\mathbf{\Omega}_2(\xi_k) = \{\frac{3\pi}{2}, \frac{\pi}{9}, \frac{2\pi[k-1]}{3}\}$ of the principal axis system of the quadrupole tensor. The calculations used the Larmor frequency $\nu_0 = 54.24$ MHz (left column) and $\nu_0 = 67.80$ MHz (right column).

3. Experimental

In order to demonstrate the usefulness of the techniques developed in this paper we have applied central transition spin-echo and inversion-recovery ^{17}O NMR spectroscopy to characterize the oxygen disorder in the silica (SiO_2) polymorph cristobalite. This system is interesting in the context of anisotropic relaxation because it is difficult or impossible to characterize the oxygen motion unambiguously by studying the fully relaxed central transition ^{17}O NMR lineshapes [40]. It is known that silica may exist in several structural modifications that are stable at different temperatures and pressures [43]. The stable crystalline forms at ambient pressures are known as quartz, tridymite, and cristobalite. The cristobalite polymorph is stable from 1743 K to its melting point at 1983 K. The silica modifications are built from SiO_4 tetrahedra sharing each of their corners with other tetrahedra to form a regular framework structure. The arrangement of the tetrahedra is different in each modification, giving the structures unique physical characteristics. The conversion of one polymorphic form into another involves the breaking of strong bonds and is a very sluggish process. This explains why the high temperature and pressure modifications may exist metastably at ambient temperatures and pressures and are found in various earth minerals. There are at least two different modifications of each polymorphic form that are stable at different temperatures and pressures. The interconversion of these forms merely involves slight rotations of the SiO_4 tetrahedra relatively to one another without any rearrangement of bonds and is an easy and reversible process. In the case of cristobalite the rotations responsible for the transition from the low-temperature α-phase to the high-temperature β-phase have been identified and shown to corres- pond to adjacent tetrahedra rotating in opposite directions.

The structural and motional details of cristobalite have previously been investigated using a variety of experimental and computational techniques. The results of these studies have led to many different models of the

α–β phase transition and been subject to much controversy. It is known from XRD experiments that β-cristobalite has a disordered structure with the oxygen atoms distributed among six or twelve positions [44,45]. However, because XRD only provides a time- and space-averaged structure it is impossible to determine the nature of the disorder. Another approach based on electron diffraction suggests that α-cristobalite has a highly twinned structure with large twin domains corresponding to different orientations of the oxygen atoms [46]. The twin domains have been observed to become smaller with increasing temperature and eventually disappear in β-cristobalite. It has been suggested that the twin domains may exist on a unit cell length scale and that β-cristobalite represents a space average of these domains [47,48]. However, recent neutron total scattering studies indicate that the intermediate range structure of β-cristobalite is not an average of α-cristobalite domains [49]. The low energy rotations in β-cristobalite have been characterized by molecular dynamics calculations and shown to correspond to excitation of rigid unit modes [50,51]. In this approach the rotations of the oxygen atoms are explained by superposing rigid unit modes on one another. This model is supported by the results of ^{17}O NMR which show that the oxygen atoms in β-cristobalite are dynamically disordered [40,52]. However, because the central transition spin-echo ^{17}O NMR spectra of cristobalite are difficult to interpret it is useful to investigate the oxygen relaxation to obtain a more accurate description of the dynamic disorder and the α–β phase transition.

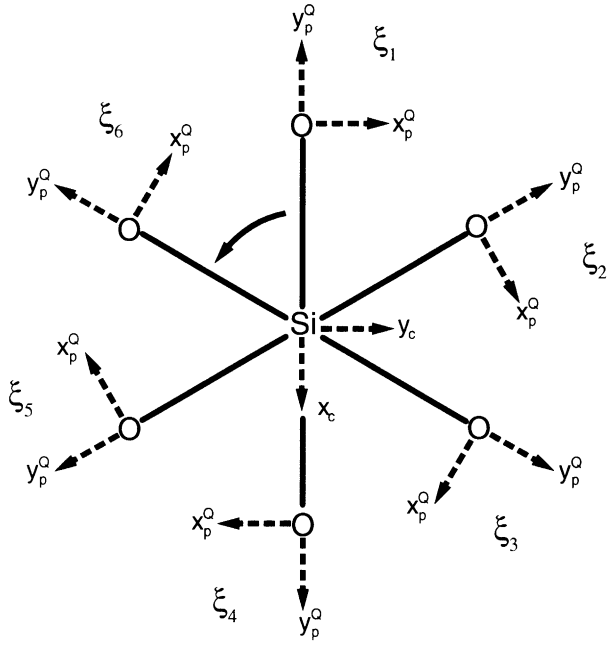

Fig. 17. Geometry of sixfold rotation of the oxygen atoms in cristobalite showing the orientations of the principal axis system of the quadrupole tensor relative to the crystallite fixed axis system.

The local disorder in cristobalite is represented by the model shown in Fig. 17 where the oxygen nuclei are distributed among $N = 6$ equally probable positions on a circle orthogonal to the Si–Si axis between adjacent tetrahedra. It is important to note that any model with $N \geqslant 3$ represents a physically plausible model of the oxygen disorder in cristobalite. However, the use of $N = 6$ is supported by the symmetry of the system as determined by XRD results [44,45]. The motion is assumed to involve transitions between nearest orientations. These transitions are described by a discrete Markov process with rate constants $k_{n,n+1} = k_{n+1,n} = k$ $(n = 1, \ldots, N-1)$ and $k_{1N} = k_{N1} = k$. In this model the lineshapes obtained for different numbers of orientations may be identical whereas the rate constants increase with the number of orientations. This shows that the rate constants are model dependent parameters and should be interpreted accordingly. Because the motional graph of the system exhibits C_{Nv} symmetry it is possible to obtain symmetrized coherences and alignments corresponding to the irreducible representations [53]. This result is useful because the evaluation of the spectral densities becomes more efficient by implementing symmetrized coherences and alignments.

The central transition spin-echo ^{17}O NMR spectra of cristobalite are shown in Fig. 18 for different tempera-

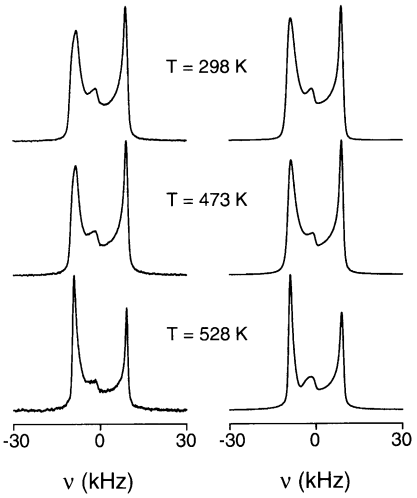

Fig. 18. Experimental (left column) and simulated (right column) central transition spin-echo ^{17}O NMR spectra of enriched (47%) polycrystalline cristobalite as function of temperature. The spectra were acquired on a Varian CMX Infinity spectrometer with Larmor frequency $\nu_0 = 54.23$ MHz, rf field strength $\nu_{rf} = 23.8$ kHz, pulse lengths $\tau_{p1} = 3.5\,\mu$s and $\tau_{p2} = 7.0\,\mu$s, and delay length $\tau_{d1} = 50\,\mu$s. There are no effects of oxygen motion below the α–β phase transition ($T < 528$ K) where the lineshapes are defined by the quadrupole and shielding interactions. The spectra exhibit significant effects of finite rf pulse length. The lineshape is different above the α–β phase transition ($T \geqslant 528$ K) where the spectral components become narrower and the intensity in the central part decreases slightly. These effects are the results of motional averaging and the decrease in the quadrupole asymmetry parameter.

tures both below and above the α–β phase transition. It is evident that there are no easily discernible effects of molecular motion in the spectra of α-cristobalite. However, the spectra show significant intensity distortions because of finite pulse length. These distortions have been accurately reproduced in the numerical simulations. The experiments were performed on highly polycrystalline samples and the spectra show no distortions related to imperfect powders. The immediate conclusion is that α-cristobalite is either a static structure or the motion is sufficiently slow ($k \leqslant 10^3$ Hz) that there are no significant lineshape effects. However, the spectra of β-cristobalite can only be simulated correctly by assuming that the oxygen atoms exhibit fast motion ($k \geqslant 10^5$ Hz). The lineshapes are defined by a motionally averaged quadrupole and shielding interaction. This implies that the rate constants cannot be determined precisely from the fully relaxed spectra. Another complication is that the fast oxygen motion makes the determination of the structural NMR parameters difficult. The most imminent problem is that the quadrupole coupling constant depends on the orientation of the quadrupole tensor used in the motional model. This is most easily understood by considering Fig. 19 where the central transition spin-echo ^{17}O NMR spectra of cristobalite are shown for different quadrupole coupling constants and tensor orientations. It is seen that the width of the spectra for slow motion is sensitive to the value of the quadrupole coupling constant. However, in the case of fast oxygen motion it is possible to define many combinations of quadrupole coupling constants and tensor orientations that produce almost identical spectra. In particular, it is seen that the width of the spectra is invariant making it impossible to determine the quadrupole coupling constant and tensor orientation.

In order to resolve the difficulties in describing the structure and motion of cristobalite it is useful to investigate the anisotropic relaxation of the oxygen nuclei. This is most conveniently accomplished by implementing the central transition inversion-recovery experiment. The partially relaxed central transition ^{17}O NMR spectra are shown in Figs. 20–23 for temperatures both below and above the α–β phase transition. The results reveal that the relaxation of the oxygen nuclei is slow in α-cristobalite and increases only slowly with temperature. Because the sample has been prepared synthetically and contains only few paramagnetic impurities the relaxation is dominated by the quadrupole and shielding interactions. The fully relaxed lineshapes of α-cristobalite exhibit no evidence of molecular motion. This observation combined with the very small but increasing relaxation rate indicates that the oxygen atoms in

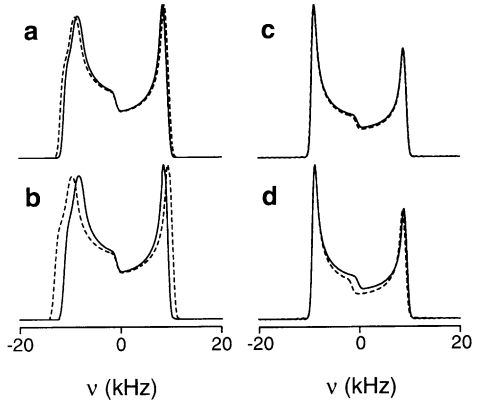

Fig. 19. Simulated central transition spin-echo ^{17}O NMR spectra of polycrystalline cristobalite. The motion involves reorientation between six orientations $\Omega_2(\xi_k) = \{\frac{3\pi}{2}, \theta, \frac{\pi[k-1]}{3}\}$ of the principal axis system of the quadrupole tensor. The lineshapes represent (a,b) slow and (c,d) fast oxygen motion. The solid lines have been calculated with the quadrupole coupling constant $C_Q = 5.35$ MHz and tensor orientation $\theta = \frac{3\pi}{180}$ while the dashed lines are for (a,c) $C_Q = 5.50$ MHz and $\theta = \frac{7\pi}{180}$ and (b,d) $C_Q = 5.75$ MHz and $\theta = \frac{12\pi}{180}$.

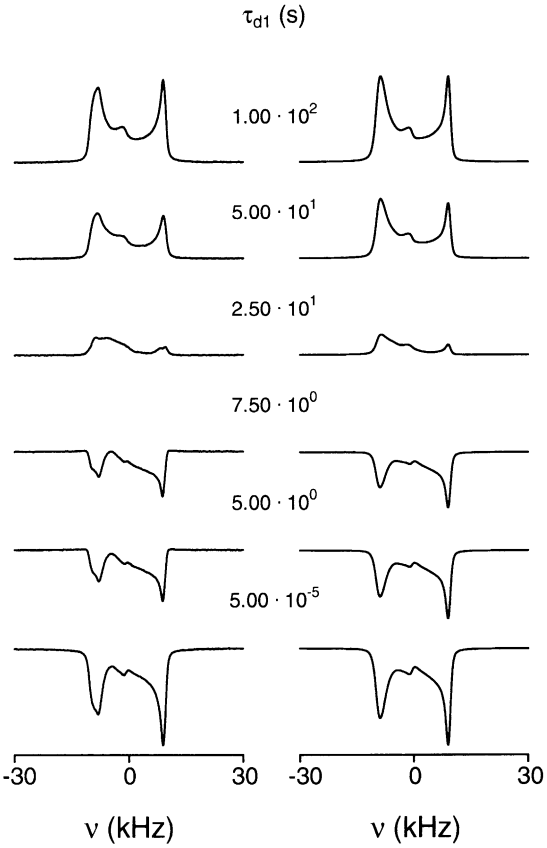

Fig. 20. Experimental (left column) and simulated (right column) central transition inversion-recovery ^{17}O NMR spectra of enriched (47%) polycrystalline cristobalite at the temperature $T = 298$ K. The spectra were recorded as function of the length τ_{d1} of the relaxation delay on a Varian CMX Infinity spectrometer with Larmor frequency $\nu_0 = 54.23$ MHz, rf field strength $\nu_{rf} = 23.8$ kHz, pulse lengths $\tau_{p1} = 7.0\,\mu$s, $\tau_{p2} = 3.5\,\mu$s, and $\tau_{p3} = 7.0\,\mu$s, and delay length $\tau_{d2} = 50\,\mu$s. The results are consistent with slow ($\log(k) = 3.50$) oxygen motion. The simulations include the effects of finite rf pulse length.

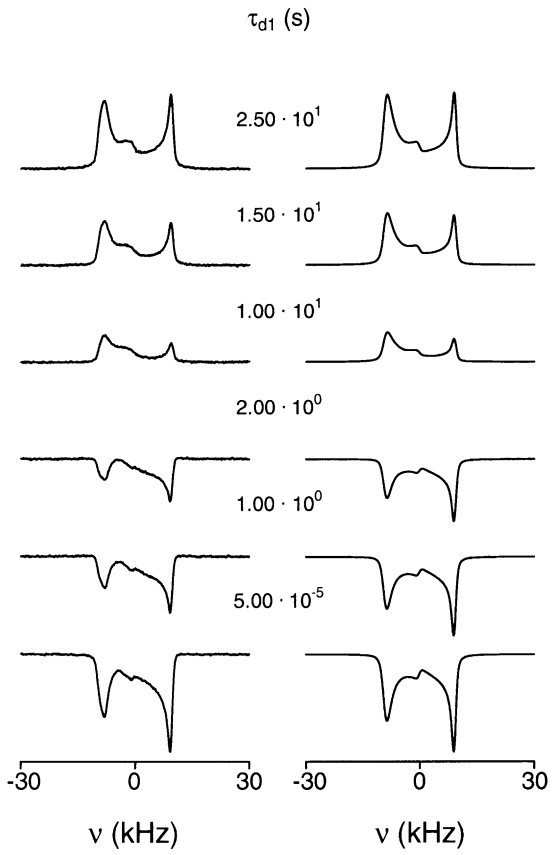

Fig. 21. Experimental (left column) and simulated (right column) central transition inversion-recovery ^{17}O NMR spectra of enriched (47%) polycrystalline cristobalite at the temperature $T = 473$ K. The results are consistent with slow ($\log(k) = 3.95$) oxygen motion.

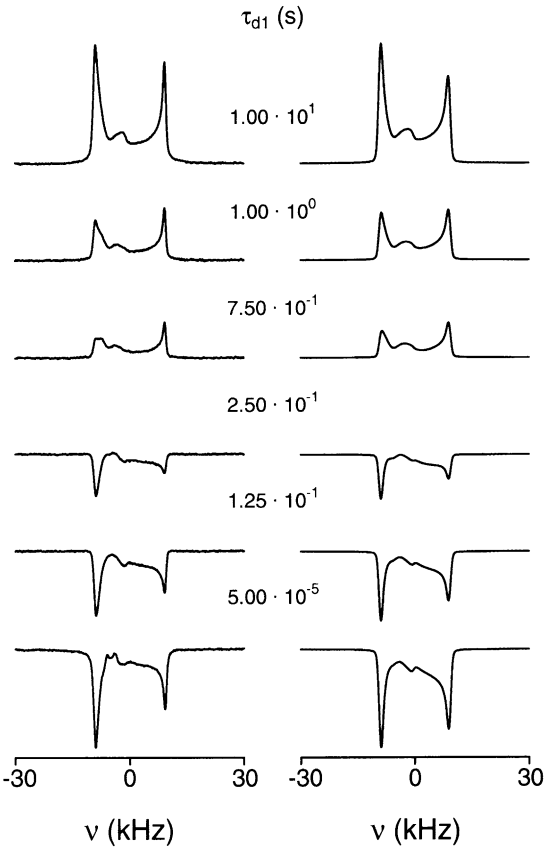

Fig. 22. Experimental (left column) and simulated (right column) central transition inversion-recovery ^{17}O NMR spectra of enriched (47%) polycrystalline cristobalite at the temperature $T = 528$ K. The spectra were simulated assuming fast ($\log(k) = 5.80$) oxygen motion.

α-cristobalite are in the slow motion regime. The results are accurately described by an Arrhenius equation with activation energy $E_a = 7.3\,\mathrm{kJ\,mol^{-1}}$ and preexponential factor $\ln(A) = 11.0$. The small activation energy indicates that the motion is almost unrestricted in α-cristobalite. The slow but increasing oxygen motion is reflected in the small but increasing relaxation rate.

The fully relaxed spectra of β-cristobalite are defined by the motionally averaged quadrupole and shielding interactions. This makes it impossible to determine the rate constants from the fully relaxed lineshapes. However, the partially relaxed spectra are sensitive to the values of the rate constants and tensor orientations. The only difficulty is that the spectra may be simulated equally well assuming either fast ($\log(k) = 5.80 \pm 0.05$) or ultrafast ($\log(k) = 11.25 \pm 0.05$) motion. This complication derives from the fact that the system has a relaxation maximum. In order to distinguish between fast and ultrafast motion it is useful to investigate the frequency dependence of the relaxation. However, an equally efficient but less expensive approach is based on the already well established observation that the relaxation rate in β-cristobalite decreases as function of temperature [52]. This indicates that the system is above its relaxation maximum and exhibits ultrafast oxygen motion. The ultrafast motion is consistent with the estimated oscillation frequencies of the rigid unit modes [50,51]. The rate constants previously obtained from fully relaxed spectra [40] are similar to those derived in this study assuming fast oxygen motion. However, because the relaxation of the oxygen nuclei can only be described correctly by ultrafast motion this demonstrates the difficulty in interpreting fully relaxed lineshapes. The fully relaxed spectra for fast and ultrafast motion are identical and the distinction can only be made by studying the partially relaxed spectra. At the α–β phase transition the motion of the oxygen atoms becomes faster by orders of magnitude. This provides an efficient relaxation mechanism and leads to motionally averaged lineshapes.

The central transition ^{17}O NMR spectra of cristobalite have been simulated with the structural and motional parameters listed in Tables 8 and 9. The results reveal several interesting details about the structure and dynamics of cristobalite. The spectra have been calculated with the ^{17}O quadrupole coupling constant

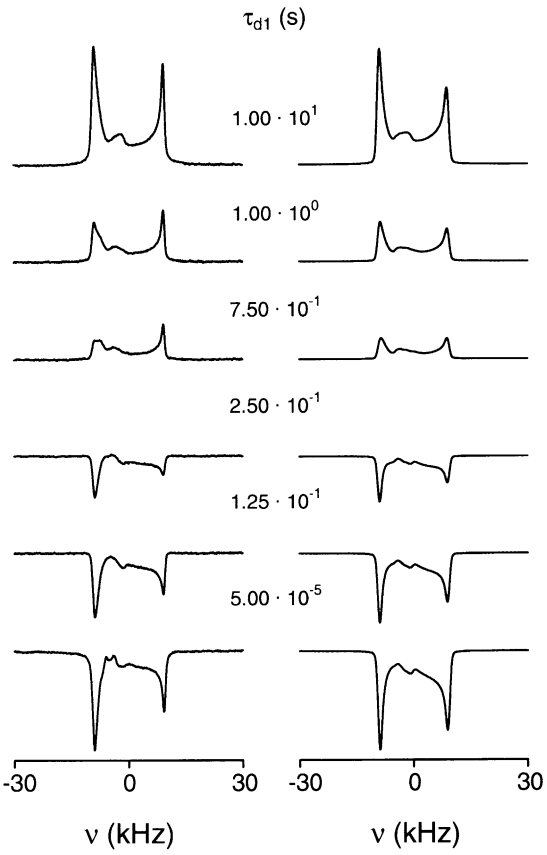

Fig. 23. Experimental (left column) and simulated (right column) central transition inversion-recovery ^{17}O NMR spectra of enriched (47%) polycrystalline cristobalite at the temperature $T = 528\,K$. The spectra were simulated assuming ultrafast ($\log(k) = 11.25$) oxygen motion.

$C_Q = 5.35\,MHz$. This value is consistent with previous results obtained by ignoring any motion of the oxygen atoms [52]. However, the quadrupole coupling constant is smaller than previously deduced from fully relaxed spectra assuming fast oxygen motion [40]. This inconsistency derives from the fact that the quadrupole coupling constant depends on the orientation of the quadrupole tensor used in the motional model. More specifically, if the principal z-axis of the quadrupole tensor is not aligned parallel to the rotation axis the width of the motionally averaged spectra will be smaller than if the principal z-axis is aligned parallel to the rotation axis. The result is that the quadrupole coupling constant is larger if the principal z-axis is not aligned parallel to the rotation axis. Because there are many combinations of quadrupole coupling constants and tensor orientations that produce the same fully relaxed spectra (Fig. 19) it is impossible to obtain the quadrupole coupling constant and tensor orientation and characterize the fully relaxed spectra. However, by measuring the relaxation anisotropy it is possible to determine the precise tensor orientation resulting in the correct value of the quadrupole coupling constant. This demonstrates the importance of acquiring partially relaxed lineshapes. The fact that the quadrupole coupling constant is close to the value previously obtained by ignoring any motion is the result of the principal z-axis being aligned close to the rotation axis. This is illustrated in Fig. 24 where the principal axis systems of the quadrupole and shielding tensors are shown relative to the crystallite fixed axis system.

Table 8
Cristobalite ^{17}O quadrupole and shielding parameters as function of temperature. The isotropic chemical shift is referenced to H_2 ^{17}O

T (K)	C_Q (MHz)	η_Q	C_S (ppm)	η_S	δ_{iso} (ppm)
298	5.35 ± 0.05	0.15 ± 0.05	50.0 ± 5.0	0.10 ± 0.10	40.5 ± 0.5
473	5.35 ± 0.05	0.15 ± 0.05	50.0 ± 5.0	0.10 ± 0.10	40.5 ± 0.5
528	5.35 ± 0.05	0.03 ± 0.05	50.0 ± 5.0	0.10 ± 0.10	40.5 ± 0.5

Table 9
Rate constant for symmetric sixfold oxygen motion and orientation of the principal axes of the cristobalite ^{17}O quadrupole and shielding tensors as function of temperature

T (K)	$\mathbf{\Omega}_1$ (rad)	$\mathbf{\Omega}_2$ (rad)	$\log(k)$
298	$\left\{\frac{3\pi}{2}, \frac{7\pi}{180} \pm \frac{\pi}{180}, \frac{\pi}{2}\right\}$	$\left\{\frac{3\pi}{2}, \frac{5\pi}{180} \pm \frac{\pi}{180}, \frac{\pi[n-1]}{3}\right\}$	3.50 ± 0.05
473	$\left\{\frac{3\pi}{2}, \frac{15\pi}{180} \pm \frac{\pi}{180}, \frac{\pi}{2}\right\}$	$\left\{\frac{3\pi}{2}, \frac{5\pi}{180} \pm \frac{\pi}{180}, \frac{\pi[n-1]}{3}\right\}$	3.95 ± 0.05
528	$\left\{\frac{3\pi}{2}, \frac{15\pi}{180} \pm \frac{\pi}{180}, \frac{\pi}{2}\right\}$	$\left\{\frac{3\pi}{2}, \frac{3\pi}{180} \pm \frac{\pi}{180}, \frac{\pi[n-1]}{3}\right\}$	11.25 ± 0.05

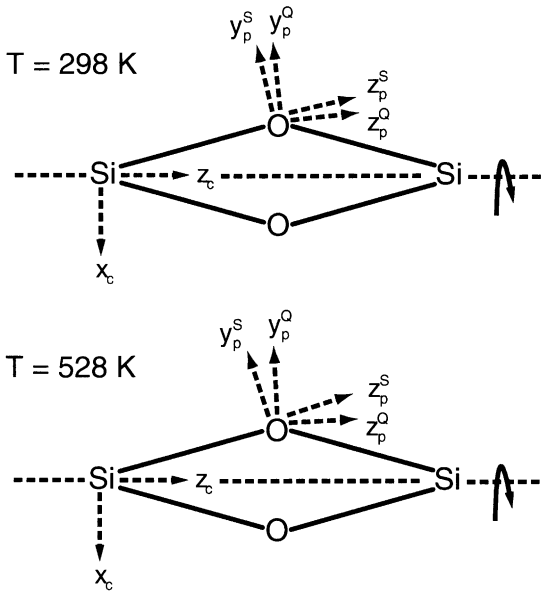

Fig. 24. Geometry of sixfold rotation of ^{17}O in cristobalite showing the orientation of the principal axis systems of the quadrupole and shielding tensors relative to the crystallite fixed axis system.

In the case of α-cristobalite the calculations used the relatively small ^{17}O quadrupole asymmetry parameter $\eta_Q = 0.15$. This value agrees with already published results for framework oxygen in similar Si–O–Si linkages [54–57]. The quadrupole asymmetry parameter decreases at the α–β phase transition and for β-cristobalite it is found that $\eta_Q = 0.03$. This effect has previously been observed and attributed to the onset of fast oxygen motion [52]. However, the motionally averaged spectra cannot be simulated using average quadrupole parameters [40]. By including the oxygen motion in the simulations the measured quadrupole asymmetry parameter reflects the inherent electronic structure of the system. This implies that the system must be subject to small structural modifications producing an almost axially symmetric local electron distribution. The most likely explanation is that the Si–O–Si angle increases slightly at the α–β phase transition. This is supported by empirical correlations between the quadrupole asymmetry parameter of framework oxygen and the Si–O–Si angle [54–57]. Similar results suggest that the quadrupole coupling constant should increase at the α–β phase transition. However, the structural change is evidently too small to be reflected in the measured quadrupole coupling constant.

The experimental spectra can only be simulated if the ^{17}O anisotropic shielding interaction is included in the calculations [40,52]. The lineshapes were simulated with the ^{17}O shielding constant $C_S = 50.0$ ppm and isotropic chemical shift $\delta_{iso} = 40.5$ ppm which are representative of similar framework structures [54–57]. The measured ^{17}O shielding asymmetry parameter $\eta_S = 0.10$ indicates that cristobalite has an almost symmetric electron distribution. This is consistent with the small quadrupole asymmetry parameter. Because of the ultrafast oxygen motion the spectra of β-cristobalite are completely insensitive to the anisotropic shielding. This has previously led to the determination of a much smaller shielding constant in β-cristobalite [40]. Although this is consistent with the lineshapes there is no other indication that the shielding constant should decrease at the α–β phase transition. As shown in Fig. 24 the orientation of the principal axis system of the shielding tensor is almost identical to the orientation of the principal axis system of the quadrupole tensor.

In order to probe the value of the Si–O–Si angle we have obtained ^{29}Si NMR spectra of cristobalite at different temperatures. These spectra are useful because the ^{29}Si isotropic chemical shift is sensitive to the precise value of the Si–O–Si angle. The results shown in Fig. 25 reveal several interesting details about the structure of cristobalite. In the case of α-cristobalite it is seen that the ^{29}Si isotropic chemical shift is constant as a function of temperature indicating an almost invariant structure. The value is consistent with results for similar framework structures and suggests that the Si–O–Si angle is in the range 140°–150° [58]. However, the ^{29}Si isotropic

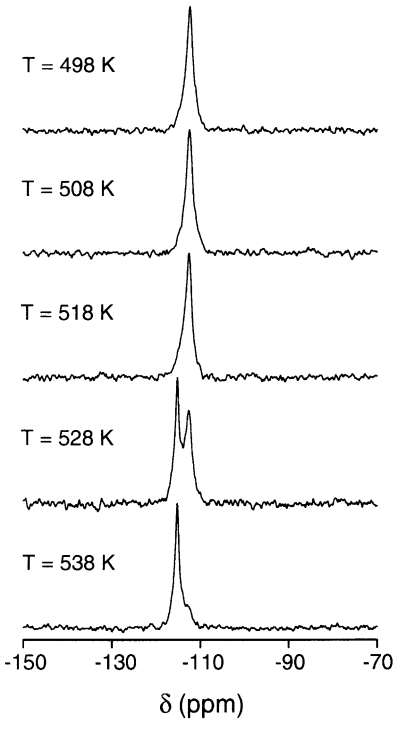

Fig. 25. Experimental ^{29}Si NMR spectra of polycrystalline cristobalite as function of temperature. The isotropic chemical shift is constant below the α–β phase transition ($T < 528$ K) indicating an invariant structure. Above the α–β phase transition ($T \geqslant 528$ K) the isotropic chemical shift decreases slightly suggesting an increase in the Si–O–Si angle.

chemical shift decreases slightly at the α–β phase transition. This reflects a structural modification involving a small increase in the Si–O–Si angle. The ^{17}O isotropic chemical shift provides another sensitive measure of the Si–O–Si angle that is consistent with the ^{29}Si isotropic chemical shift.

4. Summary

In this paper we have developed new theoretical and experimental techniques to study the effects of anisotropic relaxation and motion on fully and partially relaxed central transition NMR spectra of half-integer quadrupole nuclei. The results include a theoretical formalism based on density operator algebra and the stochastic Liouville–von Neumann equation [31–33]. This formalism may be used to describe the evolution of the density operator in the presence of molecular motion and relaxation. The effects of the nuclear spin interactions are represented by the Hamiltonian while the motion is described by a stochastic operator. The density operator formalism represents the most efficient way to simulate coherence transfer processes during periods of rf irradiation and represent finite rf pulse length effects. As shown in this paper the effects of finite rf pulse length may be substantial in selective experiments and must be included in simulations of central transition spectra. The anisotropic nuclear spin interactions fluctuate randomly in the presence of molecular motion and may stimulate the relaxation of the system [22–25]. The relaxation depends on the form of the Hamiltonian and the details of the motion and is represented by a relaxation operator. This is derived from second-order perturbation theory and involves the spectral densities of the system [24,25]. Although this formalism is valid only for small time intervals it may be used recursively to obtain the density operator at any time and for any motional regime.

There are several experimental methods that may be used to study the relaxation characteristics of half-integer quadrupole nuclei. Because these systems often have substantial quadrupole interactions it is difficult to excite the satellite transitions and the spectra are usually acquired by recording the central transition selectively [37–39]. In this paper we have used central transition inversion-recovery spectroscopy to measure the anisotropic relaxation of the different multipole alignments. In this technique the system is subject to a central transition inversion pulse creating a nonequilibrium state of multipole alignments. This state is allowed to relax in a variable relaxation period before being monitored by the central transition spin-echo sequence. The experiment is repeated for different relaxation delays to acquire a series of partially relaxed central transition lineshapes.

The simulation of central transition inversion-recovery spectra involves describing the relaxation of the different nuclear spin multipole alignments. For half-integer quadrupole nuclei the $2I$ multipole alignments may be classified into $I+\frac{1}{2}$ odd-rank and $I-\frac{1}{2}$ even-rank multipole alignments. The most important interactions for half-integer quadrupole nuclei are the quadrupole and shielding interactions. For these interactions the relaxation of the odd-rank alignments is defined by $I+\frac{1}{2}$ simultaneous equations while the relaxation of the even-rank alignments is specified by a system of $I-\frac{1}{2}$ equations. It is important to note that the simultaneous evolution of the multipole alignments is consistent with nonexponential relaxation. This has largely been ignored in the literature where most investigations have focused on systems with vanishing higher rank multipoles for which the relaxation may be approximately exponential [22]. However, it is evident that the higher rank multipole alignments cannot be ignored for large quadrupole interactions.

In order to understand the combined effects of anisotropic relaxation and motion the theoretical formalism has been used to calculate central transition ^{17}O NMR spectra for different systems. The results have revealed several important details about relaxation of half-integer quadrupole nuclei. It has been shown that partially relaxed lineshapes acquired using central transition inversion-recovery spectroscopy are highly sensitive to the precise values of the rate constants and the orientations of the quadrupole tensor. This may be used to distinguish between different motional models that would otherwise produce almost identical fully relaxed lineshapes. The only limitation is that it is often possible to define several models for which the partially relaxed lineshapes are indistinguishable. However, an eminent advantage is that the number of possible models is reduced significantly. It is found that slow and intermediate molecular motion may be identified by the small relaxation rate and characteristic lineshape effects. For systems dominated by the quadrupole interaction the relaxation rate is a decreasing function of the Larmor frequency and an increasing function of the rate constants. For the shielding interaction there is no significant frequency dependence for slow and intermediate motion. In the case of fast and ultrafast motion the spectra gradually converge to an almost invariant lineshape defined by the motionally averaged Hamiltonian. In order to distinguish between fast and ultrafast motion it is useful to exploit the fact that any system has a relaxation maximum. This implies that the relaxation rate is an increasing function of the rate constants for fast motion and a decreasing function for ultrafast motion. The quadrupole relaxation rate is independent of the Larmor frequency for ultrafast motion and a decreasing function for fast motion. The shielding relaxation rate is an increasing function of the Larmor

frequency for ultrafast motion and invariant for fast motion.

As an example the theoretical and experimental methods developed in this paper have been applied to characterize the oxygen disorder in the silica (SiO_2) polymorph cristobalite. The results of central transition spin-echo ^{17}O NMR spectroscopy are insufficient to determine all the structural and motional details of cristobalite [40,52]. There are no easily discernible effects of oxygen motion in the spectra of α-cristobalite whereas the lineshapes of β-cristobalite are consistent with either fast or ultrafast motion. This implies that α-cristobalite is either a static structure or the motion is sufficiently slow that there are no lineshape effects. Because the spectra of β-cristobalite are determined by a motionally averaged quadrupole and shielding interaction it is impossible to determine the precise values of the rate constants. Another complication is that it is impossible to obtain the value of the quadrupole coupling constant and the orientation of the quadrupole tensor from the fully relaxed spectra. In order to resolve these problems we have applied central transition inversion-recovery ^{17}O NMR spectroscopy to study the anisotropic relaxation of the oxygen nuclei. The results show that the oxygen motion in α-cristobalite is slow and increases only slowly as a function of temperature. This is reflected in the small but increasing relaxation rate and the absence of lineshape effects in the fully relaxed spectra. The partially relaxed lineshapes of β-cristobalite are shown to be consistent with ultrafast motion. This demonstrates that the motion increases by orders of magnitude at the α–β phase transition. The ultrafast motion is reflected in the large but decreasing relaxation rate and the motionally averaged lineshapes. The partially relaxed lineshapes define the correct orientation of the quadrupole tensor and corresponding value of the quadrupole coupling constant. The quadrupole asymmetry parameter is found to decrease at the α–β phase transition. This is not the result of motional averaging but may be attributed to a small structural modification involving an increase in the Si–O–Si angle. In order to investigate this model in more detail we have applied ^{29}Si NMR spectroscopy to study the structure of cristobalite. The results show that α-cristobalite has an almost invariant structure. However, at the α–β phase transition the ^{29}Si isotropic chemical shift decreases slightly indicating an increase in the Si–O–Si angle.

The experimental and theoretical methods introduced in this paper provide a general framework for measuring and characterizing motional disorder in solids. The approach is based on analyzing the combined effects of anisotropic motion and relaxation on solid-state central transition NMR spectra of half-integer quadrupole nuclei. The relaxation effects extend the accessible motional range by orders of magnitude and make it possible to investigate both ultraslow and ultrafast molecular motion. The additional constraints imposed by studying partially relaxed spectra improve the accuracy of the experiments significantly. Although partially relaxed spectra may often be simulated using many different motional models the study of anisotropic relaxation reduces the number of possibilities. The techniques are applicable to a variety of physical problems including transport measurements and studies of anisotropic molecular motion in both crystalline and amorphous solid materials. The results presented for cristobalite are consistent with the rigid unit mode model and represent the first experimental measurement of ultraslow and ultrafast oxygen motion in a solid framework structure.

Acknowledgments

This research was supported by grants from the United Kingdom Joint Infrastructure Fund (JIF) and Joint Research Equipment Initiative (JREI).

References

[1] H.W. Spiess, Adv. Polym. Sci. 66 (1985) 23.
[2] K. Schmidt-Rohr, H.W. Spiess, Multidimensional Solid State NMR and Polymers, Academic Press, London, 1994.
[3] G. Engelhardt, D. Michel, High Resolution Solid State NMR of Silicates and Zeolites, Wiley, New York, 1987.
[4] R.J. Kirkpatrick, Rev. Mineral. 18 (1988) 341.
[5] J.F. Stebbins, Rev. Mineral. 32 (1995) 191.
[6] E.C. Kelusky, C.A. Fyfe, J. Am. Chem. Soc. 108 (1986) 1746.
[7] N.J. Turro, X. Lei, W. Li, Z. Liu, M.F. Ottaviani, J. Am. Chem. Soc. 122 (2000) 12571.
[8] E. Gelerinter, Z. Luz, R. Poupko, H. Zimmermann, J. Phys. Chem. 94 (1990) 8845.
[9] G.L. Hoatson, R.L. Vold, NMR Basic Principles and Progress 32 (1994) 1.
[10] R. Poupko, E. Furman, K. Müller, Z. Luz, J. Phys. Chem. 95 (1991) 407.
[11] A.E. Aliev, K.D.M. Harris, J. Phys. Chem. 101 (1997) 4541.
[12] P.S. Sidhu, G.H. Penner, K.R. Jeffrey, B. Zhao, Z.L. Wang, I. Goh, J. Phys. Chem. 101 (1997) 9087.
[13] M.M. Woolfson, An Introduction to X-Ray Crystallography, Cambridge University Press, Cambridge, 1970.
[14] G.E. Bacon, Neutron Diffraction, Clarendon Press, Oxford, 1975.
[15] M. Mehring, High Resolution NMR in Solids, Springer, Berlin, 1983.
[16] C.A. Fyfe, Solid State NMR for Chemists, CFC Press, Guelph, 1983.
[17] A.D. Becke, Phys. Rev. 38 (1988) 3098.
[18] C. Lee, W. Yang, R.G. Parr, Phys. Rev. 37 (1988) 785.
[19] K. Wolinski, J.F. Hilton, P. Pulay, J. Am. Chem. Soc. 112 (1990) 8257.
[20] G. Ciccotti, D. Frenkel, I.R. McDonald, Simulation of Liquids and Solids. Molecular Dynamics and Monte Carlo Methods in Statistical Mechanics, North-Holland, Amsterdam, 1987.

[21] R.J. Wittebort, E.T. Olejniczak, R.G. Griffin, J. Chem. Phys. 86 (1987) 5411.
[22] H.W. Spiess, NMR Basic Principles and Progress 15 (1978) 55.
[23] D.A. Torchia, A. Szabo, J. Magn. Reson. 49 (1982) 107.
[24] A. Abragam, Principles of Nuclear Magnetism, Oxford University Press, London, 1961.
[25] A.G. Redfield, Adv. Magn. Reson. 1 (1965) 1.
[26] B. Halle, Prog. Nucl. Magn. Reson. Spectrosc. 28 (1996) 137.
[27] A. Wokaun, R.R. Ernst, J. Chem. Phys. 67 (1977) 1752.
[28] B.C. Sanctuary, Mol. Phys. 48 (1983) 1155.
[29] G. Campolieti, B.C. Sanctuary, H.B.R. Cole, J. Magn. Reson. 88 (1990) 457.
[30] W. Nosel, S. Capuani, D. Capitani, F. DeLuca, J. Magn. Reson. 150 (2001) 178.
[31] U. Fano, Rev. Mod. Phys. 29 (1957) 74.
[32] R. Kubo, Fluctuation, Relaxation, and Resonance in Magnetic Systems, Oliver and Boyd, Edinburgh, 1962.
[33] J.H. Kristensen, G.L. Hoatson, R.L. Vold, Solid State Nucl. Magn. Reson. 13 (1998) 1.
[34] J.H. Kristensen, H. Bildsøe, H.J. Jakobsen, N.C. Nielsen, Prog. Nucl. Magn. Reson. Spectrosc. 34 (1999) 1.
[35] C.W. Gear, Numerical Initial Value Problems in Ordinary Differential Equations, Prentice-Hall, Englewood Cliffs, New Jersey, 1971.
[36] J.H. Kristensen, G.L. Hoatson, R.L. Vold, J. Comp. Phys. 170 (2001) 415.
[37] A. Samoson, E. Kundla, E. Lippmaa, J. Magn. Reson. 49 (1982) 350.
[38] A. Samoson, E. Lippmaa, Phys. Rev. 28 (1983) 6567.
[39] P.R. Bodart, J.P. Amoureux, Y. Dumazy, R. Lefort, Mol. Phys. 98 (2000) 1545.
[40] J.H. Kristensen, I. Farnan, J. Chem. Phys. 114 (2001) 9608.
[41] M. Witschas, H. Eckert, H. Freiheit, A. Putnis, G. Korus, M. Jansen, J. Phys. Chem. 105 (2001) 6808.
[42] R.W. Schurko, S. Wi, L. Frydman, J. Phys. Chem. 106 (2002) 51.
[43] H.D. McGaw, Crystal Structures. A Working Approach, W.B. Saunders, London, 1973.
[44] D.R. Peacor, Z. Cristallogr. 138 (1973) 274.
[45] F. Wright, A.J. Leadbetter, Philos. Mag. 31 (1975) 1391.
[46] R.L. Withers, J.G. Thompson, T.R. Welberry, Phys. Chem. Miner. 16 (1989) 517.
[47] T.R. Welberry, G.L. Hua, R.L. Withers, J. Appl. Crystallogr. 22 (1989) 87.
[48] B.M. Hatch, S. Ghose, Phys. Chem. Miner. 17 (1991) 554.
[49] D.A. Keen, M.T. Dove, J. Phys.: Condens. Matter 11 (1999) 9263.
[50] K.D. Hammonds, M.T. Dove, A.P. Giddy, B. Winkler, V. Heine, Am. Mineral. 81 (1996) 1057.
[51] M. Gambhir, M.T. Dove, V. Heine, Phys. Chem. Miner. 26 (1999) 484.
[52] D.R. Spearing, I. Farnan, J.F. Stebbins, Phys. Chem. Miner. 19 (1992) 307.
[53] J.H. Kristensen, I. Farnan, J. Chem. Phys. 270 (2001) 109.
[54] H.K.C. Timken, G.L. Turner, J.P. Gilson, L.B. Welsh, E. Oldfield, J. Am. Chem. Soc. 108 (1986) 7231.
[55] H.K.C. Timken, N. Janes, G.L. Turner, S.L. Lambert, L.B. Welsh, E. Oldfield, J. Am. Chem. Soc. 108 (1986) 7236.
[56] I. Farnan, P.J. Grandinetti, J.H. Baltisberger, J.F. Stebbins, U. Werner, M.A. Eastman, A. Pines, Nature 358 (1992) 31.
[57] X. Xue, J.F. Stebbins, M. Kanzaki, Am. Mineral. 79 (1994) 31.
[58] F. Mauri, A. Pasquarello, B.G. Pfrommer, Y.G. Yoon, S.G. Louie, Phys. Rev. 62 (2000) 4786.